Title: Wave impacts on structures with rectangular geometries: Part 2 Decks, Baffles and Seawalls with impermeable or porous surfaces

Authors: Nor Aida Zuraimi **Md Noar,** Matthew **Elliott-Sands** and Martin **Greenhow**
Affiliation: Department of Mathematics, Brunel University, Uxbridge, UB8 3PH, UK.
Corresponding author: Martin Greenhow, Department of Mathematical Sciences, Brunel University, Uxbridge, UB8 3PH, UK. mastmmg@brunel.ac.uk, +44 1895-265622

Highlights

A simplified analytical model allows rapid exploration of the effect of wave impact on decks and baffles within different rectangular geometries with free, impermeable or porous boundaries.

Pressure impulses, impulses and moment impulses are presented.

Wave impacts on structures with rectangular geometries: Part 2 Decks, Baffles and Seawalls with impermeable or porous surfaces

Nor Aida Zuraimi **Md Noar**[1] **,** Matthew **Elliott-Sands** and Martin **Greenhow**
Department of Mathematics, Brunel University, Uxbridge, UB8 3PH, UK.
aidaz@ump.edu.my , Matthew.Elliott-Sands@brunel.ac.uk,
martin.greenhow@brunel.ac.uk

Abstract
This paper considers wave impacts on baffles, on baffles or decks adjacent to a vertical wall, and on porous seawalls and/or sea beds. For seawalls and vertical baffles, impacts can occur in steep waves, whilst a deck can be struck from below by a rising wave crest either in open sea or in a tank with standing waves (sloshing). A simple analytical model for the pressure impulse, *P*, due to a wave of idealized geometry and dynamics is developed and applied to the following geometries with impermeable surfaces:

1. horizontal wave impact onto a vertical wall with a deck at the waterline,
2. vertical wave impact under a deck in the same configuration (equivalent to vertical water impact of a horizontal plate),
3. horizontal wave impact onto a surface-piercing vertical baffle in open sea,
4. as for 3. but with the baffle in front of a wall,
5. as for 4. but with a deck extending from the vertical wall to the baffle,
6. bottom-mounted baffle in front of a wall with impact occurring on the wall.

We also consider cases that complement part 1 of this paper to include the effect on impacts on a seawall with a porous sea bed and/or sea wall with/without a berm. Finally we reconsider case 3) above but with a porous baffle.

The method uses eigenfunction expansions in each of the rectangular regions that satisfy some of the impermeable or porous surface conditions, and a simplified free-surface condition. Their unknown coefficients are determined from the impact boundary condition, impermeable or porous boundary conditions and by matching the solutions, in any two neighbouring rectangles, along their common boundary. Although the fluid motion is treated rather crudely, the method yields the pressure impulse throughout the entire region. Impulses, *I*, and moment impulses, *M*, on all or parts of the structure are also presented.

Keywords: wave impact, baffles, slamming, seawall impact, deck impact, sloshing, oscillating water column, porosity, porous seabed

---

[1] Funded by research grant FRGS (Vote No. RDU140108) from Ministry of Higher Education of Malaysia and Research and Innovation Department of Universiti Malaysia Pahang (UMP).

Present address: Fakulti Sains dan Teknologi Industri, Universiti Malaysia Pahang, Lebuhraya Tun Razak, 26300 Gambang, Kuantan, Pahang, MALAYSIA.

1. Introduction

Wave impact or slamming is of major concern to the integrity of ships, coastal and offshore structures, and in accelerated vehicle-mounted tanks. A brief literature review is given by Md Noar, and Greenhow (2015), part I of this paper, which models impacts of short duration (typically 10^{-2}s or less) and high peak pressure (typically $4\text{x}10^5$ Nm^{-2}). Such impacts are thought to be particularly dangerous for the lower decks of offshore rigs. However, engineers cannot simply raise those decks without incurring great costs, especially in accommodating the increased overturning moments on the structure. For coastal engineers, the survival of seawalls with/without berms was considered in part 1; here we consider additional structures such as decks and baffles mounted on or nearby the seawall. We also consider the effect of seawall and berm porosity, which is shown to reduce the impact loads and therefore provides engineers with the option of designing porous, rather than impermeable, structures. Seabed porosity also reduces loads on the seawall, but pressure and pressure gradients on the seabed may affect the foundations; our results could form input states for subsequent fluid penetration during impact and to assess the likelihood of liquefaction of the seabed material. Equally importantly, in partially-filled tanks, for example in LNG carriers, fuel or liquid cargo tanks, and in many industrial situations, baffles are often used to damp out sloshing waves and so can be subject to the same type of wave impacts. Again, baffle porosity is shown to be beneficial in reducing impact loads. The baffles and/or parts of the tank wall can be impacted either by steep waves in the case of low filling, or standing wave crests hitting horizontal boundaries, in the case of high filling. Impacts on baffles and decks are also relevant to oscillating water column wave energy devices in 'survival mode' i.e. in rough seas where no energy is extracted and the turbine is bypassed by having either a fully-ventilated chamber or a closed water-filled chamber.

Given the complexity of the wave climate in the open ocean and the diversity of sloshing modes that can occur in a tank, see Faltinsen and Timokha (2014) for an extensive review, some sort of simplification is needed to allow a model that is sufficiently simple for engineering use and rapid examination of the effect of different impact, geometrical and porosity parameters. Numerical simulations that include the development of waves and their impacts exist, see e.g. Kim (2001), Brizzolara S. *et al* (2009), Koli and Kulkarni (2010), Ming (2010) and Wang and Xiong (2014) but require sophisticated treatment because the time scales of the wave motion and impact phenomena are very different, making direct simulations expensive. Fortunately a simplifying feature is that the most violent impacts occur when the wave fronts are closely aligned with the structure, so that the fluid motion predominantly occurs in the two-dimensional vertical plane normal to the structure. Moreover, these 2D solutions could also be used in "strip theory" approximations for 3D problems where the geometry or boundary conditions vary relatively slowly in the z-direction compared with those in the x-y plane considered here.

Accordingly, we here extend Cooker and Peregrine's (1990) simplified 2D model of pressure impacts to study impact on a seawall, giving the local and global impulsive loads and moments, see also Cooker and Peregrine (1995). Their model is based on the pressure

impulse, defined in Lamb (1932) as the pressure at any point integrated over its (short) duration from just before impact (at t_b) to just after (at t_a) i.e.

$$P(\mathrm{x},\mathrm{y}) = \int_{t_b}^{t_a} p(x,y,t)dt \approx \frac{\Delta t\, p_{peak}}{2} \qquad [1]$$

Clearly $P = 0$ on the free surface. Lamb shows that the gradient of P is the fluid density times the velocity change during the impact; this gives the impermeable boundary and impact conditions shown in figure 1, and this is further discussed for porous boundaries in sections 8 and 9. The approximate equality in Eq. [1] assumes a triangular rise to, and fall from, the pressure peak during the impact time, Δt (this is not part of our model and must be given). Cooker (1990) shows that for short duration impacts, P satisfies Laplace's equation and that its gradient is simply the difference of the fluid velocity before and after impact. Thus the model requires no information about the precise nature of the impact. Hofland *et al* (2010) carried out very large-scale tests of impact and showed that those due to entrapping of an air pocket in an overturning wave give rise to smaller peak impact pressures than those arising from 'flip through' where a trough in front of an overturning wave fills from the bottom by forming a rapid vertical jet. Nevertheless, they showed that with suitable values of the impact region (μ, see below) and estimates of Δt, which are much larger for entrapped air pocket case (30 and 90 ms) than for 'flip through' (0.5 and 15 ms), values of maximum wall pressures were reasonably consistent with those of Cooker and Peregrine for both types of impact. This gives us a rationale for using the calculated values of P, with a suitable estimate or measurement of Δt that takes the nature of the impact into account, to estimate peak pressures throughout the fluid region. This applies even for cases 1 and 2 where the dynamics of the impact are more complicated in nature, as discussed by Kisacik *et al* (2012 & 2014).

Recently, Chen *et al* (2019) have incorporated pressure impulse theory with subsequent wave forces on a wall with overhang, here considered in cases 1 and 2. In their introduction, those authors give a detailed account of the considerable uncertainties faced by engineers and provide a rationale for splitting the two phases of wave-structure interaction: impact, using the pressure impulse, and subsequent wave forces. Although they use experimental data for their impulse calculations, they could have measured the impact velocity and impact region and used Md Noar (2012) results. Other possible uses of the current theory might include estimating the transient responses of structures due to initial impact (Chen *et al* say that maximum forces can occur after the impact due to dynamic amplification), crack initiation and propagation in the impact zone region and possible short-duration liquefaction of the seabed which could compromise the integrity of the whole structure. Before such projects are attempted, it is very desirable that experimenters validate the current models and this will require reporting of impact velocity and impact zone geometry. This is seldom done, but seems feasible with high-speed cameras and PIV velocity measurements.

Cooker and Peregrine solve (analytically) the problem of impact on a seawall using an expansion of eigenfunctions, each of which satisfies Laplace's equation and all of the boundary conditions apart from those at the seawall, where a Fourier method gives its coefficient. The method is very efficient, allowing for rapid examination of the effect of

different impact sizes and velocity profiles. Part 1 extended this model to consider a seawall with a berm, ditch or with a missing block, where similar eigenfunction expansions in each rectangular region are matched at their mutual boundary, giving a matrix equation for the unknown coefficients. This paper applies a similar approach, with suitably modified eigenfunctions, to study impact on the geometries specified in the abstract. Once the coefficients are known, the impulses and moment impulse are found analytically by term-by-term integration of the expansions.

For all problems considered, the normal velocity profile in the impact region is assumed constant (U_0) and to the impacted surface, whilst the wave surface is assumed to be parallel to the impacted surface. (There is no constraint on the velocity component tangential to the impact surface.) Other choices of normal velocity profile were considered by Cooker (1990) and would be possible to implement for any of the problems of this paper. This additional complication would, however, add little to the realism of the model unless more is known about the impacting wave (perhaps from PIV experiments). In reality, engineers are likely to know only the water depth and an estimate of the impact speed, probably taken as the phase speed of the wave ($U_0 \approx \sqrt{gH}$ in shallow water). The top free surface of the wave is assumed to be flat in all cases, as in Fig. 1, Fig. 6 and the contour plots given below which also show the geometry considered with the engineered part of the structure being drawn in a heavy line.

The boundary-value problems are non-dimensionalised as follows: lengths by division by the water depth H and velocities by U_0. Results are given in non-dimensional form throughout, but physical quantities (denoted by a prime) can be easily recovered by: $P' = P\,\rho U_0 H$, $I' = \rho U_0 H^2 I$ and $M' = \rho U_0 H^3 M$ for the pressure impulse, impulse and moment impulse respectively. As mentioned above, all three quantities could be important in the engineering context; the P might initiate and propagate cracks whilst the I and M are global loads that might damage, or even destroy a structure, for example by breaking off decks or baffles. The effect of having porous boundaries is shown to be beneficial for the engineered structure, but seabed porosity may degrade the integrity of foundations.

2. Case 1: impact on a wall under a deck

The boundary-value problem considered is summarized in Fig. 1. The geometry of the wave is idealized with the impact region being vertical (the sloping line denoting the impact region is simply a schematic) and the fluid filling the rectangular region $0 < x < b_2$, $-1 < y < 0$. Thus the wave is thought of as being long and with a vertical front face, and passes just under the projecting deck before striking the vertical wall of the structure. This rather specialized situation is nevertheless relevant since Kisacik *et al* (2012) measured the most severe impacts on both wall and deck when the air gap between the crest of the impacting wave and deck was small, see also Kisacik *et al* (2014) who present an empirical formula for the effect of the air gap size. However, their experiments measure two impacts; the wave impacting the wall, and the subsequent vertical jet impacting the deck. So whilst not directly comparable, the case considered here could be viewed as an extreme form of impact, although experiments or fully-nonlinear calculations would be needed to check

such a claim. Unfortunately the results of Kisacik *et al* (2012) do not allow direct comparison of even the impact on the wall, since the impacted regions in their experiments on the wall and the deck are not identical to the present case (they have an air gap under the deck and so the wall/deck impacts are not simultaneous). Furthermore, since they do not measure representative impact velocities, they non-dimensionalise by the hydrostatic pressure by $\rho g H_1$ where H_1 is the trough-to-crest wave height (whereas we neglect gravity). Using $U_0 \approx \sqrt{gH}$ as above, gives their non-dimensional pressure maximum as $\frac{p'_{max}}{\rho g H_1} \approx \frac{2PH}{\Delta t H_1}\sqrt{\frac{H}{g}}$. Using values from their most extreme impacts and assuming that the wave height is approximately equal to the water depth at the toe of their wall (0.1m) and that the impact duration is twice their rise time (0.3 ms), gives extreme P values of 0.05 - 0.1. Although not in agreement, these values are at least consistent with the values of 0.3 - 0.5 shown in Fig. 2 below for our more extreme case.

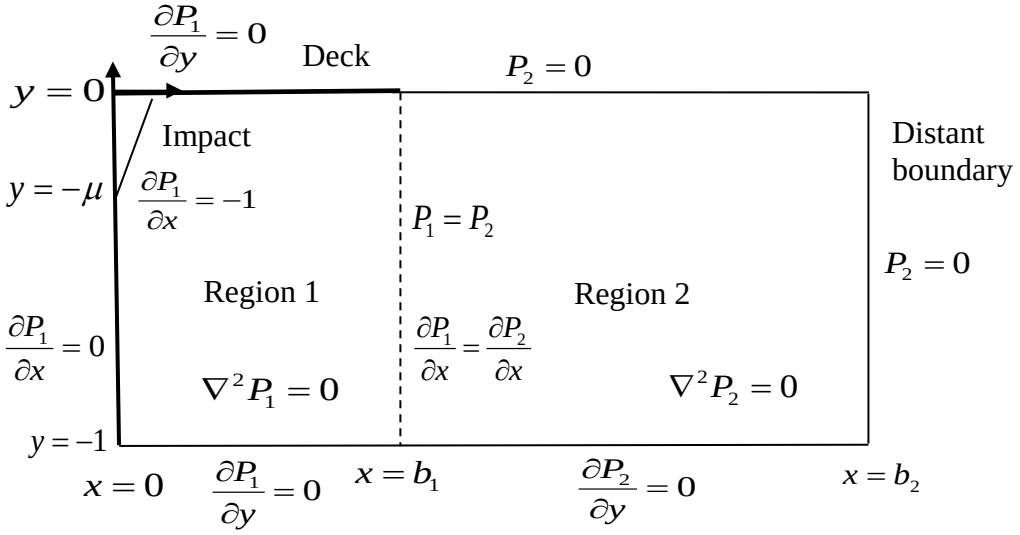

Fig. 1 Non-dimensional boundary-value problem for the pressure impulse for impact over the upper part of a wall just below the deck.

Because the condition at $y = 0$ changes at the end of the deck ($x = b_1$), it is necessary to split the problem into two regions and match P and its normal derivative across their mutual boundary ($x = b_1$, $-1 < y < 0$). Since P satisfies Laplace's equation in each region, second and higher derivatives are also continuous across the common boundary. The pressure impulse in each region can be written using eigenfunction expansions; for the problems considered in this paper, we use the form given by Cox and Cooker (1999), but other forms are possible. Thus in region 1 we write:

$$P_1(x,y) = Ax + C + \sum_{n=1}^{\infty} \cos(\gamma_n y)\left\{\alpha_n \frac{\cosh(\gamma_n(x-b_1))}{\cosh(\gamma_n b_1)} + \beta_n \frac{\sinh(\gamma_n(x-b_1))}{\sinh(\gamma_n b_1)}\right\} \quad [2]$$

where $\gamma_n = n\pi$ so that the deck condition is automatically satisfied. Note the inclusion of terms in both cosh and sinh since no far-field boundary condition applies here, and the 'secular' terms $Ax+C$ which also satisfy the deck and seabed conditions in addition to Laplace's equation. Beyond the deck (region 2), the expansion is:

$$P_2(x,y) = \sum_{n=1}^{\infty} c_n \sin(\lambda_n y) \frac{\sinh[\lambda_n(x-b_2)]}{\cosh(\lambda_n b_2)} \qquad [3]$$

where $\lambda_n = (n - 1/2)\pi$. Each term here satisfies the seabed and free-surface conditions and a far-field condition at $x = b_2$. Another possibility would be to use decreasing exponentials in place of the hyperbolic functions in Eq. [3] as in Cooker (1990), but our calculations show that $b_2 = 2$ is sufficiently distant for the calculation of all quantities of interest and this is taken throughout the paper (similarly $b_1 = -2$ for section 4).

The system of equations for the unknown coefficients (α_n, β_n, c_n) is truncated at n = N, giving a 3N x 3N matrix system which is solved by:

- applying the seawall condition at $x = 0$, where we have $\frac{\partial P}{\partial x} = -1$ for $0 > y > -\mu$ and $\frac{\partial P}{\partial x} = 0$ $-\mu > y > -1$, multiplying by the set of basis functions $\cos(\gamma_l y)$ and integrating from $y = -1$ to $y = 0$ (as in the usual Fourier approach). With $l = 0$, this gives $A = -\mu$. For $l = 1, 2, \ldots$ N this gives diagonal components of the matrix in the first N rows,
- applying the continuity of pressure impulse condition across the mutual boundary at $x = b_1$, $0 > y > -1$ integrating from $y = -1$ to $y = 0$. This gives an expression for C in terms of the unknowns c_n.
- matching at N equally-spaced collocation points the pressure impulse and its horizontal derivative of P across the line at $x = b_1$, $0 > y > -1$. This gives block diagonal components of the matrix in the final 2N rows.

For further details of this procedure and its convergence, see Md Noar (2012). Typically N = 80 is sufficient for the pressure impulse to converge to about 0.1% accuracy.

For a very short deck we expect P on the wall to be unaffected by the deck and indeed when $b_1 = 0.01$, results are, except very close to the deck, indistinguishable from Cooker and Peregrine's (1990) results for all values of μ. However, for the other cases shown in Fig. 2, 3 & 4, the deck has a very significant effect on P, and I and M on the wall. As expected from the boundary conditions, the contours are orthogonal to the un-impacted lower part of the wall and the deck. I and M also increase rapidly with increasing deck length.

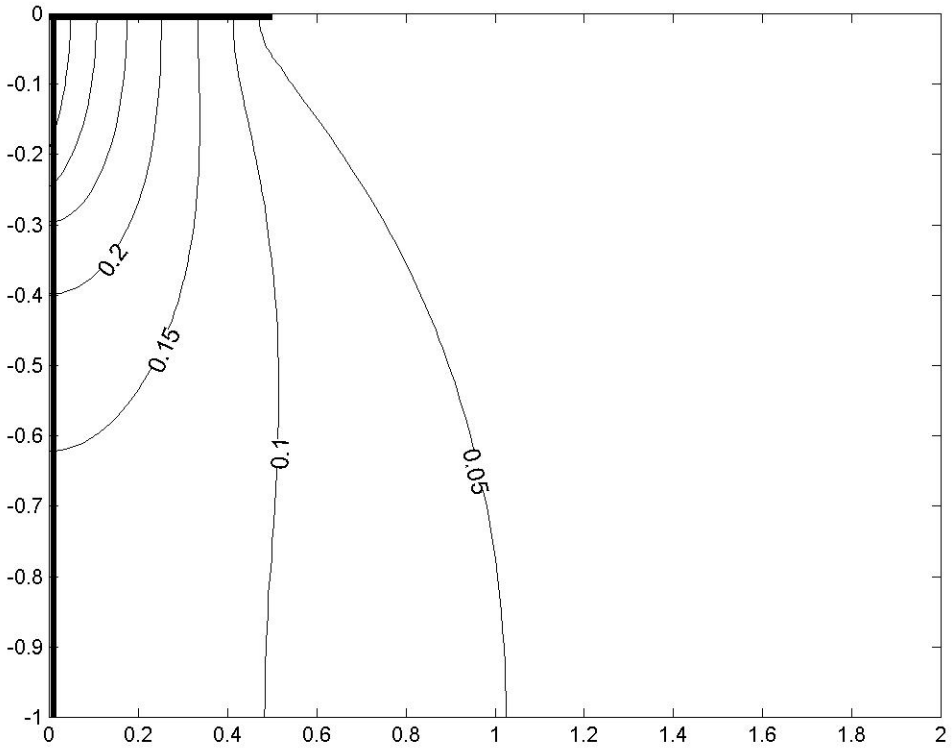

a)

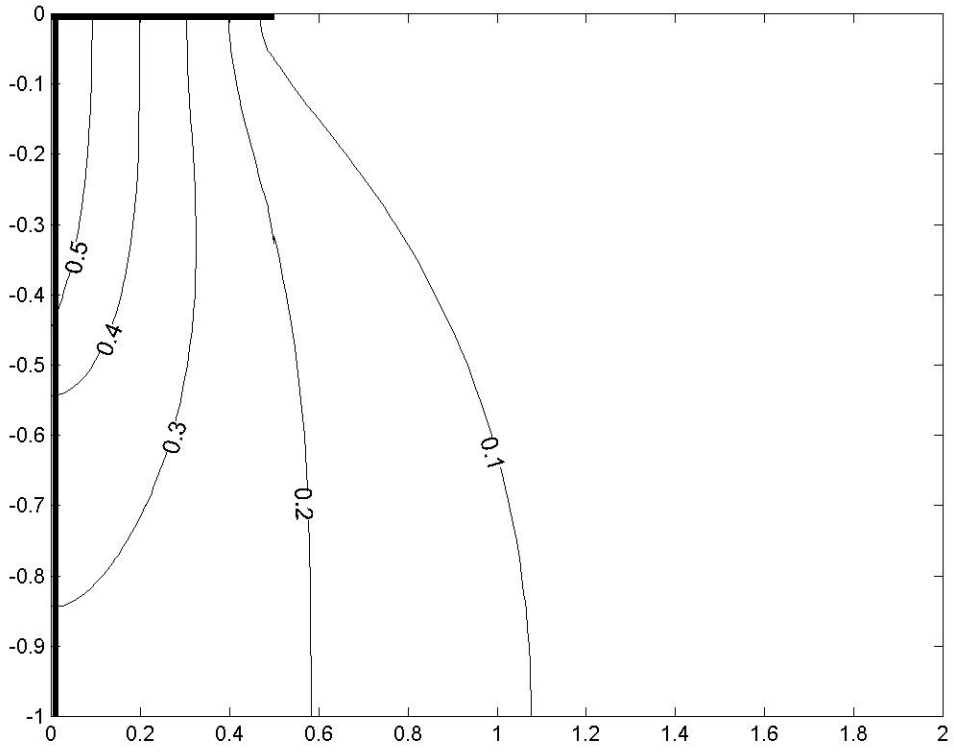

b)

Fig. 2 *P* due to wave impact on a vertical wall under a deck: $b_1 = 0.5$, a) $\mu = 0.25$, b) $\mu = 0.5$. The value of *P* on unlabeled closely-spaced contours is given by continuing the increment from neighbouring contour values.

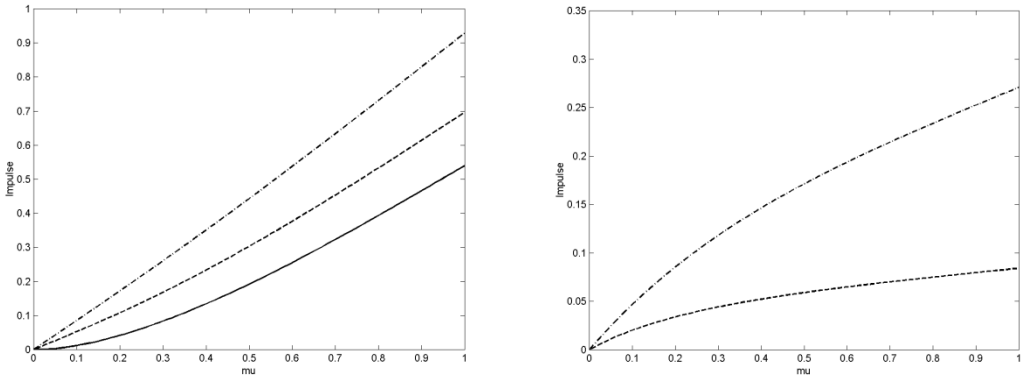

a) b)

Fig. 3 *I* due to horizontal wave attack on a vertical wall under a deck a) no deck (solid), $b_1 = 0.25$ (dashed) and $b_1 = 0.5$ (dash-dotted) and b) acting vertically upwards on the deck (right): $b_1 = 0.25$ (dashed) and $b_1 = 0.5$ (dash-dotted).

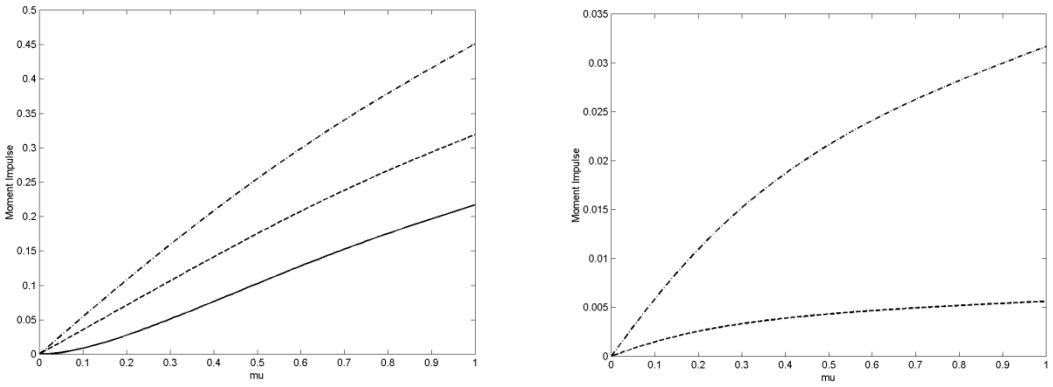

a) b)

Fig. 4 *M* due to horizontal wave attack on a vertical wall a) under a deck taken about the foot of the seawall (0,-1): no deck (solid), b_1 = 0.25 (dashed) and b_1 = 0.5 (dash-dotted) and b) on the deck (right) taken about the origin: b_1 = 0.25 (dashed) and b_1 = 0.5 (dash-dotted).

3. Case 2: impact on a deck projecting from a wall

Here the geometry is the same as that given in Fig. 1, but with no impact on the wall and the whole of the underside of the deck being impacted. Thus different boundary conditions apply on the wall and deck i.e. $\frac{\partial P_1}{\partial x} = 0$ on $x = 0, 0 > y > -1$ and $\frac{\partial P_1}{\partial y} = 1$ on $y = 0, 0 < x < b_1$. Consequently different eigenfunctions need to be chosen for region 1 as follows:

$$P_1(x,y) = A + \sum_{n=1}^{\infty} \alpha_n \cos(\gamma_n y) \frac{\cosh(\gamma_n x)}{\cosh(\gamma_n b_1)} + \beta_n sin(\lambda_n y) \frac{\cosh(\lambda_n x)}{\cosh(\lambda_n b_1)} \qquad [4]$$

The eigenfunction expansion for region 2 is given by eq. 3. The problem is solved in the same way as previously although there is now no longer a simple expression for *A* (it is a summation with terms having coefficients β_n and c_n and so, after truncation *A* can therefore be eliminated to again give an 3N x 3N system of equations). On $y = 0, 0 < x < b_1$ terms in α_n satisfy $\frac{\partial P_1}{\partial y} = 0$ whilst terms in β_n satisfy $\frac{\partial P_1}{\partial y} = 1$ and thus, as pointed out by a referee, this series could be replaced by $[(y+1)^2 - x^2]/2$, thereby reducing the system of equations to 2N x 2N. This gives results graphically identical to those in Fig. 5; in particular the maximum value of *P* i.e. *P*(0,0) = 0.5175 from either method.

This problem was considered by Wood and Peregrine (1996) for water of finite or infinite depth, using conformal mappings (here our wall is their line of symmetry). Their results for the wall and deck impulses, given in brackets below, agree well with ours. Fig. 5 shows results for a deck projecting for half of the water depth, as considered by Wood and Peregrine. As discussed below, there is a square root singularity at the end of the deck. Thus, in order to capture the strong gradients near the end of the deck (near *x* = 0.5), these results use N = 60. For b_1 = 0.25 *I* on the wall is 0.087(0.089) whilst that on

the deck is 0.049(0.050), while for $b_1 = 0.5$ the corresponding figures are 0.276(0.280) and 0.203(0.206). The maximum P values, P_{max} , which occur at the origin in both models, agree closely (0.51 versus Wood and Peregrine's 0.52). These small differences presumably arise from the present method's difficulty of resolving the steep pressure gradients due to the square root singularity at the end of the deck with sufficient accuracy, see below and also Wood and Peregrine.

Taking moments about the bottom of the wall (0,-1), M on the deck and wall are in the anticlockwise direction with values 0.005 (0.005) for the deck and 0.22 (0.23) for the wall for $b_1 = 0.25$, and 0.043 (0.044) for the deck and 0.33 (0.33) for the wall for $b_1 = 0.5$. These results are comparable to those shown in Fig. 4. Wood and Peregrine did not present results for M but these are given in brackets above using their method.

It is worth noting that although Wood and Peregrine's method is analytic, its calculation is far more expensive in computer time than that for the present method. It is therefore worth comparing with the infinite depth case. Clearly the wall acts as a line of symmetry and hence this problem is equivalent to that for the vertical impact of a flat plate into deep water, as studied by Wagner (1932) and often used in ship bottom slamming studies. Faltinsen and Timokha (2014) use such a model for slamming on the roof of a tank with extreme sloshing, whilst Faltinsen and Rognebakke (1999) include the effect of finite depth and/or side walls by including image potentials. The present case is, of course, far simpler since the width of the impacted area is not expanding, but known *a priori*. In deep water, the P is directly analogous to that of the complex flow around a flat plate in unbounded fluid, see also Wood and Peregrine (1996). Then the complex pressure impulse is simply $P + iQ = -iz + \sqrt{1 - z^2}$ where Q is the conjugate harmonic function (analogous to the stream function) and $z = x + iy$. Here, we have non-dimensionalising by the plate half-beam b_1, so $-1 \leq x \leq 1$ and $y = 0$ defines the plate. Integrating across the bottom of the plate gives I as $\pi/4 \approx 0.7854$ and the M as 1/3. When non-dimensionalised by b_1 rather than by water depth, our values for the deck I are 0.81(0.82) for $b_1 = 0.5$ and 0.78(0.79) for $b_1 = 0.25$ where Wood and Peregrine's results are again in brackets; the corresponding M values are 0.34(0.35) and 0.33(0.34). The values are therefore close to the plate values, but further reduction in b_1 or taking more terms in the eigenfunction expansion does not improve convergence, especially for the M. This is due to the rapid vertical variation in P in the above analytic solution near the end of the deck which is not present in the eigenfunction expansions; the situation is similar to Fourier analysis of a square wave where taking more terms produces the well-known Gibbs' phenomenon. For $0.25 \leq b_1 \leq 0.65$ values of I vary almost linearly from 0.78 to 0.83; the same is true for M which also varies almost linearly from 0.33 to 0.35. Both I and M show a weak depth effect. Outside this b_1 region, results are unreliable.

For this deep-water model, the corresponding values on the wall are singular i.e. integrating from 0 to $-D$ shows that I diverges logarithmically and M diverges linearly as $D \to \infty$. However, integrating over (0,-H) the infinite-depth P values (assumed to be a reasonable approximation to the finite depth case for increasing H) gives values of wall I of 0.081 for $b_1 = 0.25$ and 0.239 for $b_1 = 0.5$ (after non-dimensionalising w.r.t. the depth H). These values compare reasonably well with those above for the finite depth problem

(0.087 and 0.276 respectively) but M (0.05 for $b_1 = 0.25$ and 0.15 for $b_1 = 0.5$) do not agree with the values given above.

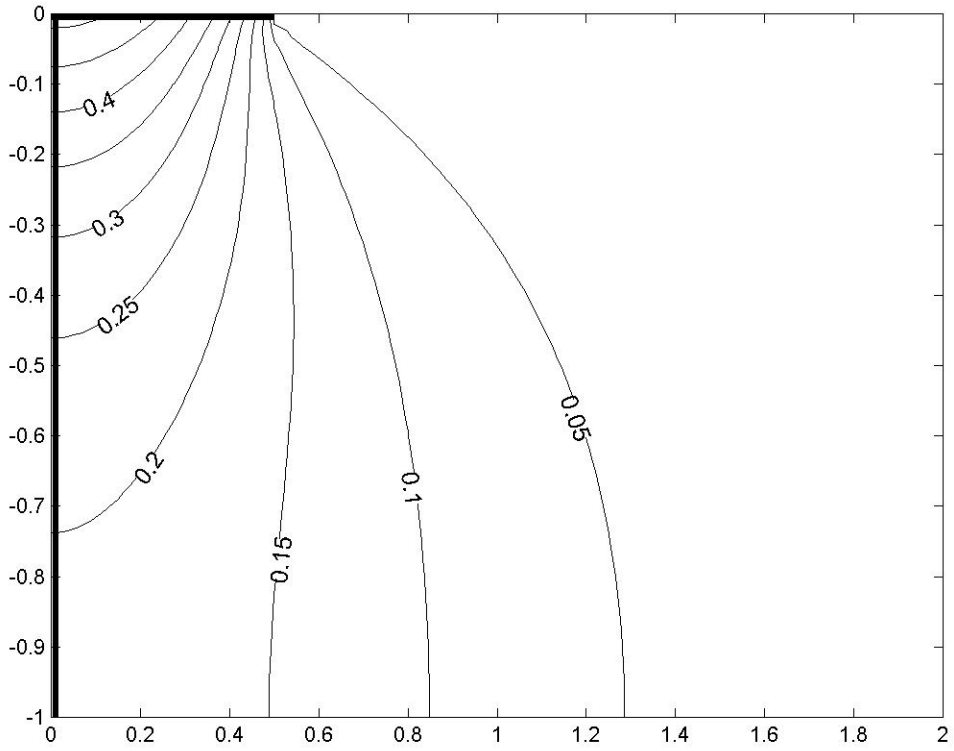

Fig. 5 P due to wave impact on a deck projecting from a wall: $b_1 = 0.5$. The value of P on unlabeled closely-spaced contours is given by continuing the increment from neighbouring contour values.

Whilst offshore or coastal engineers will be most interested in the pressure impulse on the deck and wall, and naval architects on the deck (as a model of a ship bottom slam), the whole pressure impulse field may be of interest to marine biologists since it may shed some light on why whales breach. This may be to remove parasites (deck pressure impulse) or to stun prey below them (the whole field).

4. Case 3: Horizontal wave impact onto a surface-piercing vertical baffle in open sea.

This problem has been considered by several workers; for example Chan and Melville (1988) considered a plate struck by a wave crest. However, this is not directly comparable to the situation given in Fig. 6 which has the same water depth in both regions. This is further discussed at the end of this section.

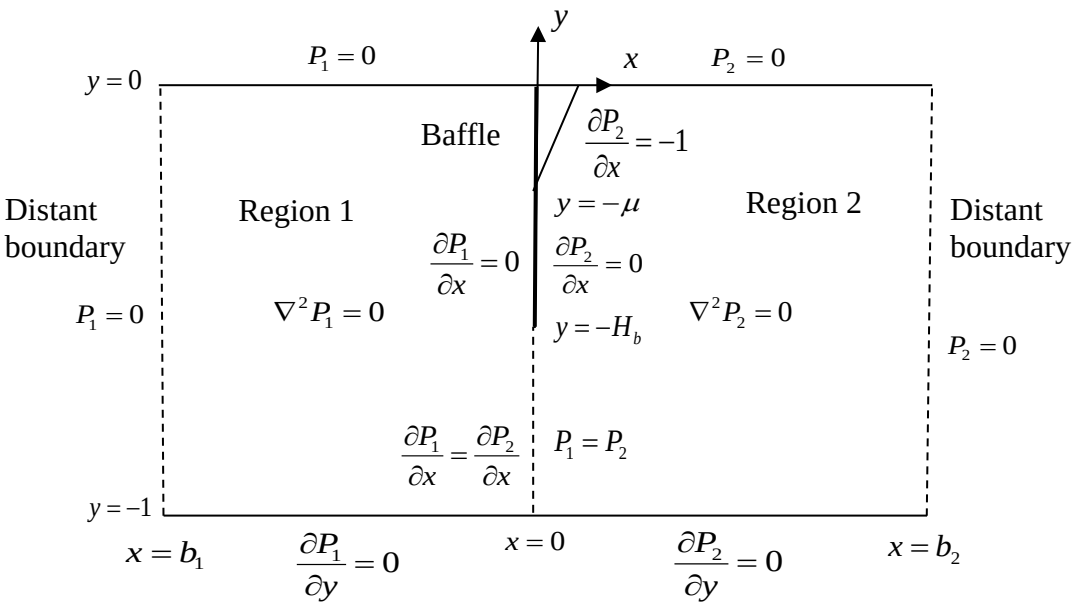

Fig. 6 Non-dimensional boundary-value problem for the pressure impulse for impact on the right-hand side of a surface-piercing baffle in open sea.

The eigenfunction representation of region 1 is simply:

$$P_1(x,y) = \sum_{n=1}^{\infty} \alpha_n \sin(\lambda_n y) \frac{\sinh[\lambda_n (x - b_1)]}{\cosh(\lambda_n b_1)} \qquad [5]$$

The eigenfunction expansion for region 2 is given by eq. 3. The problem is solved as before using a combination of Fourier and collocation methods, for details see Md Noar (2012).

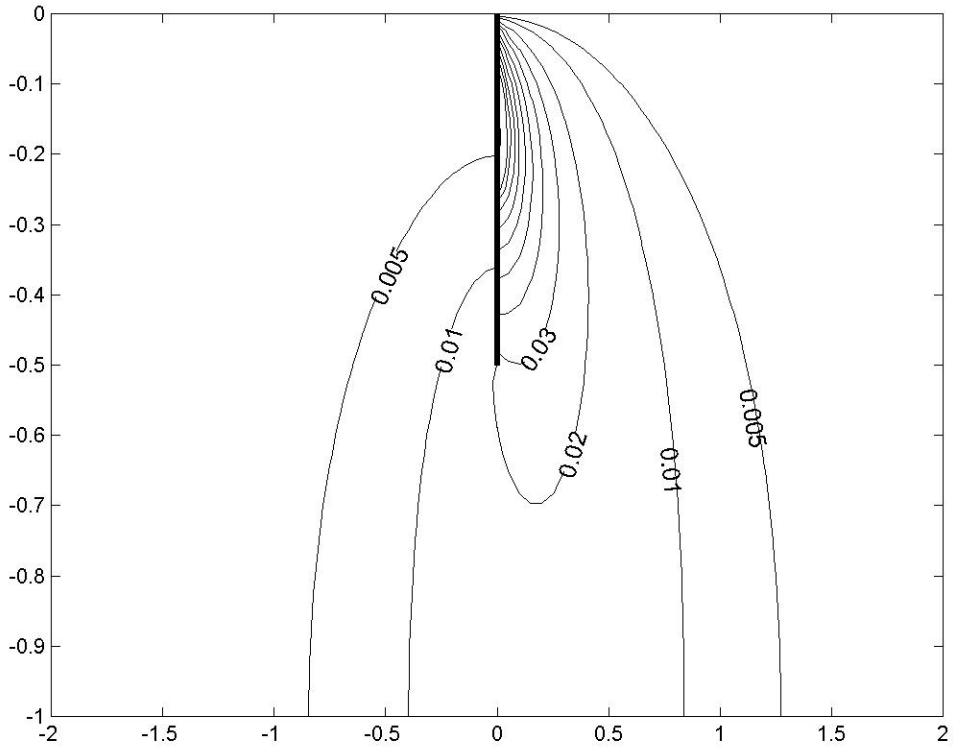
0
-0.1
-0.2
-0.3
-0.4
-0.5
-0.6
-0.7
-0.8
-0.9
-1
-2
-1.5
-1
-0.5
0
0.5
1
1.5
2
0.005
0.01
0.03
0.02
0.01
0.005

a)

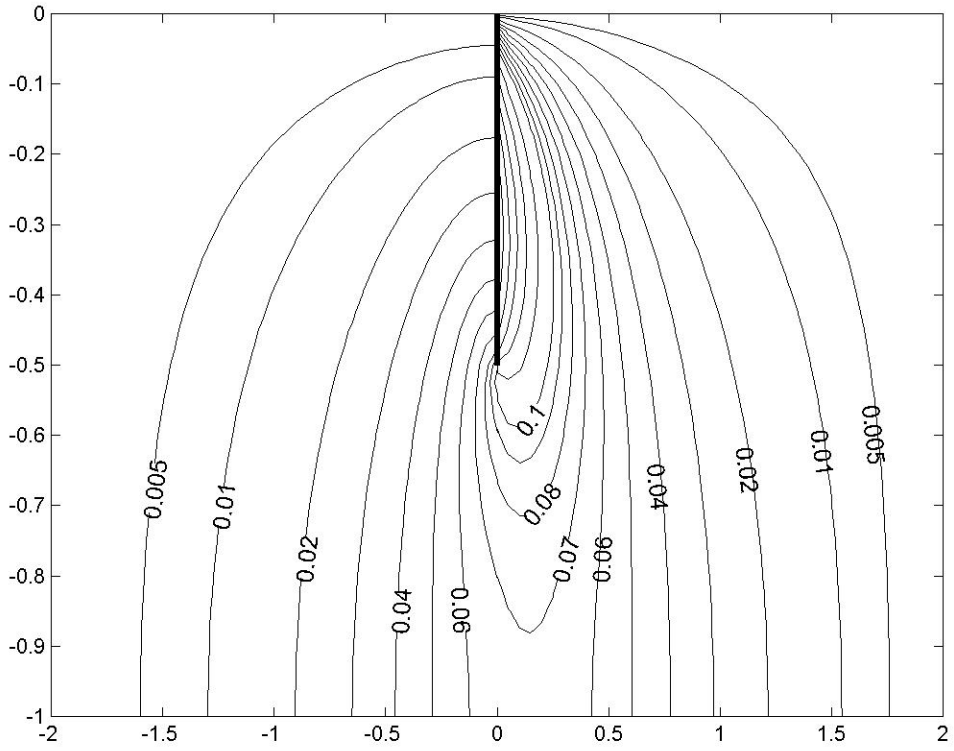
0
-0.1
-0.2
-0.3
-0.4
-0.5
-0.6
-0.7
-0.8
-0.9
-1
-2
-1.5
-1
-0.5
0
0.5
1
1.5
2
0.005
0.01
0.02
0.04
0.06
0.1
0.08
0.07
0.06
0.04
0.02
0.01
0.005

b)

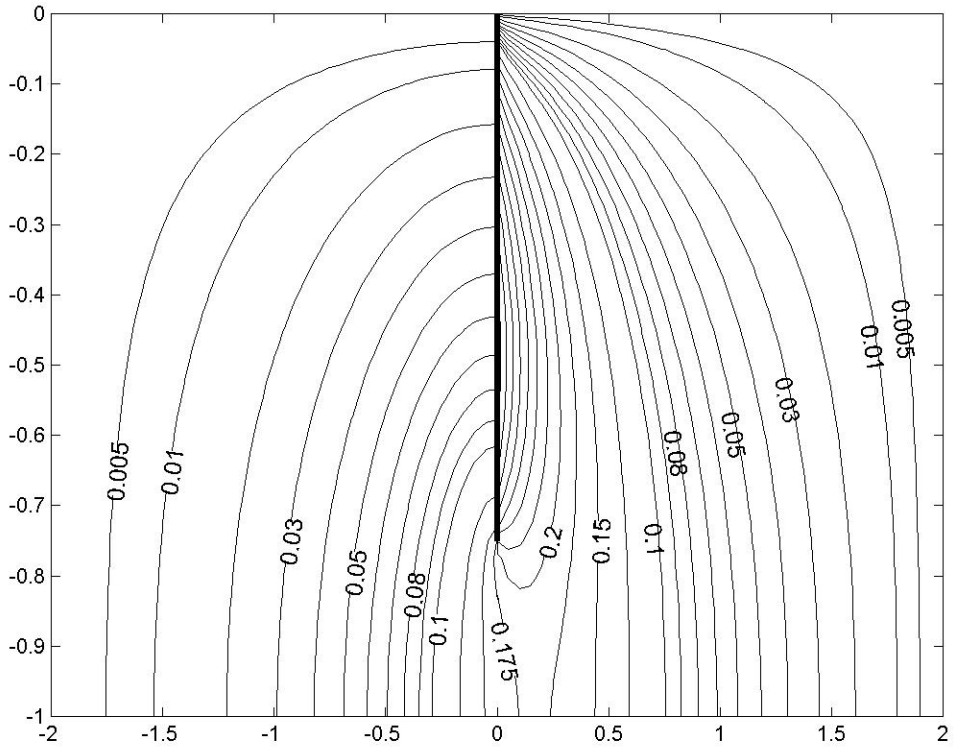

c)

Fig. 7 *P* due to wave impact on a baffle with H_b = 0.5. a) μ = 0.25, b) μ = 0.5 and c) with H_b = 0.75, μ = 0.75. The value of *P* on unlabeled closely-spaced contours is given by continuing the increment from neighbouring contour values.

The contours shown in Fig. 7 are spaced as follows: 0.005, 0.01 to 0.1 in steps of 0.01, 0.125 to 0.5 in steps of 0.025. For H_b = 0.5, μ = 0.25 P_{max} is 0.14, for H_b = 0.5, μ = 0.5 it is 0.25 and for H_b = 0.75, μ = 0.75 it is 0.39. These are generally lower than the corresponding *P* for the case of a seawall considered by Cooker and Peregrine (1990) i.e. 0.14, 0.29 and 0.47 for μ = 0.25, 0.5 and 0.75 respectively.

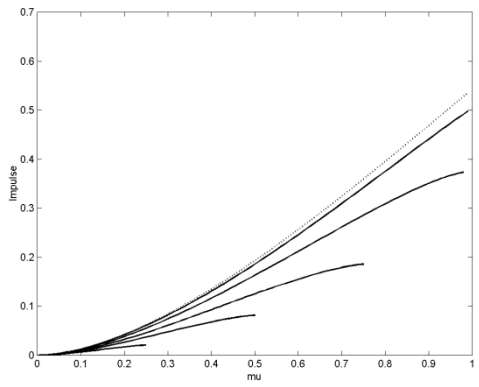

a)

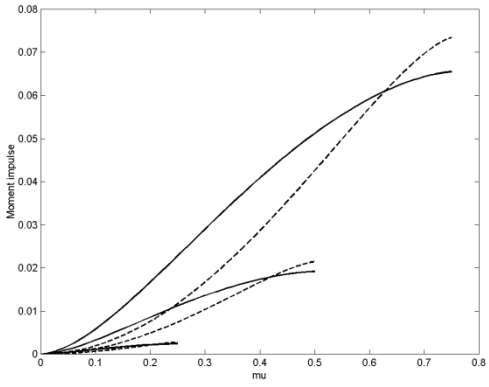

b)

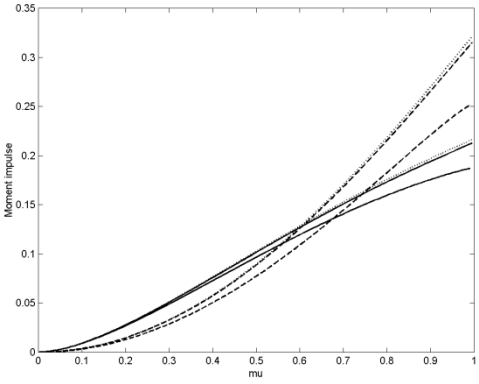

c)

Fig. 8 a) *I* due to wave impact on a baffle with H_b = 0.25, 0.5, 0.75, 0.99 and 0.995, and for the wall case (dotted) b) *M* with H_b = 0.25, 0.5, 0.75: solid/dashed line about the baffle bottom/top and c) as for b) but with H_b = 0.99 and 0.995 (bottom two solid or dashed lines) and the wall case (dotted). For convenience of plotting, the negative of *M* about the top of the baffle is shown in the figure (as dotted lines).

Fig. 8 shows that as H_b increases, I and M also increase up to the line end when the entire baffle is impacted. As H_b tends to 1, convergence to the impact results for a wall, see Md Noar and Greenhow (2015) reproduced as the dotted lines here in Figs. 8a and 8c, is exceptionally slow. For Fig. 8b the solid line shows *M* taken about the bottom of the baffle, being positive in the anti-clockwise direction, whilst the dashed lines show the negative of (the clockwise) *M* that acts at the top of the baffle at (0,0); the same convention applies to Fig. 8c. There are three factors contributing to the slow convergence to the seawall case: the pressure impulse is integrated only over the baffle not the entire water depth, the pressure impulses near the lower end of the baffle are relieved by passing under the baffle and there is an appreciable *P* field on the back of the baffle, see Md Noar (2012), that partially balances that on the front.

A referee suggested that it would be of interest to consider that case where the free surface leaves the bottom of the baffle, so that the left-hand fluid region extends

vertically from $w = -H_b$ to -1. We agree that this would better model impact from a single very large wave; in more mixed seas the left-hand fluid region might extend vertically from a new geometrical parameter w to -1 where w might be any value with $w > -1$ (even positive). Exploration of the effect of this parameter is for a future study, but we here speculate on the referee's suggested case $w = -H_b$. Then we would expect a significant increase from the results of Fig. 8 for I and M since there would be no pressure impulse on the back of the baffle to balance that on the front. One could then be tempted to simply consider P and hence I and M on the baffle front using the present calculations. Unfortunately this is likely to be in error since P on the front of the baffle would certainly decrease in this new configuration, especially near the bottom of the baffle due to the line of $P = 0$ at the bottom of the baffle. So further calculations to explore non-zero values of w are needed for cases 3 and 4 given here, and for porous baffles/seabeds considered in section 8.

5. Case 4: horizontal wave impact onto a surface-piercing vertical baffle in front of a wall.

With the origin again at the top of the baffle, the eigenfunction expansion for region 1 is now

$$P_1(x,y) = \sum_{n=1}^{\infty} \alpha_n \sin(\lambda_n y) \frac{\cosh[\lambda_n(x-b_1)]}{\cosh(\lambda_n b_1)} \qquad [6]$$

The eigenfunction expansion for region 2 is again given by eq. 3 and the solution procedure similar to that used previously, for details see Md Noar (2012).

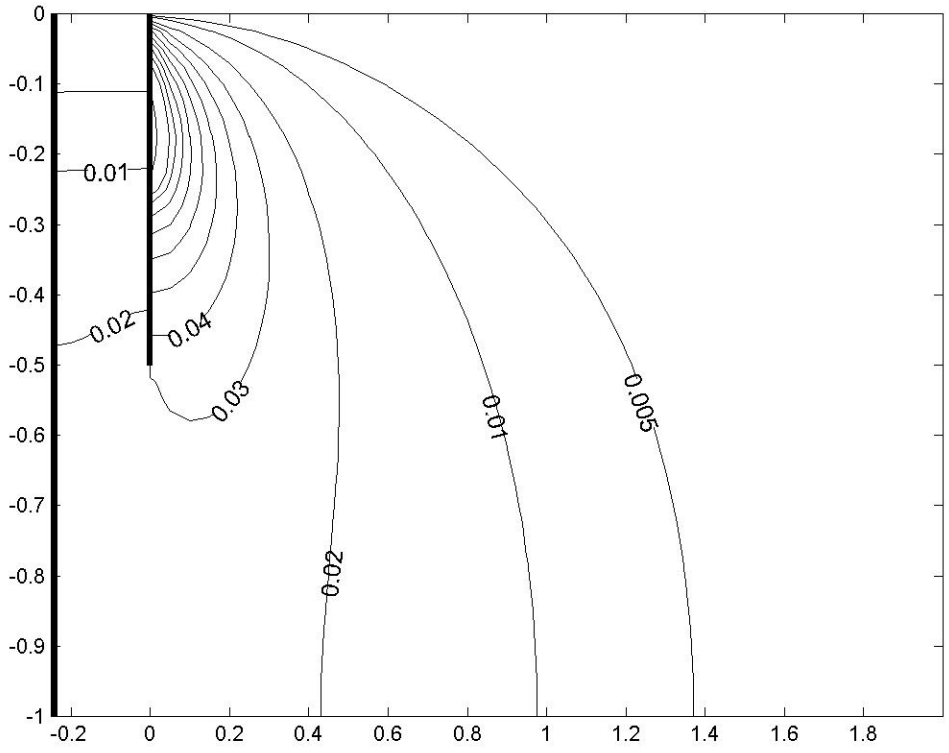
0
-0.1
-0.2
-0.3
-0.4
-0.5
-0.6
-0.7
-0.8
-0.9
-1
-0.2
0
0.2
0.4
0.6
0.8
1
1.2
1.4
1.6
1.8
0.01
0.02
0.04
0.03
0.02
0.01
0.005

a)

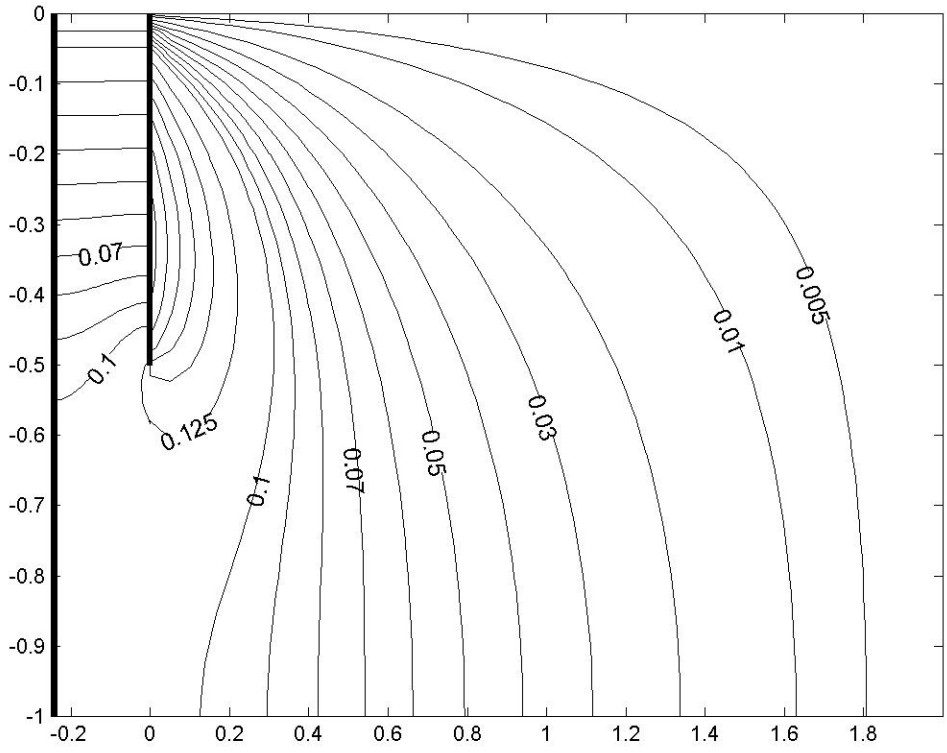
0
-0.1
-0.2
-0.3
-0.4
-0.5
-0.6
-0.7
-0.8
-0.9
-1
-0.2
0
0.2
0.4
0.6
0.8
1
1.2
1.4
1.6
1.8
0.07
0.1
0.125
0.1
0.07
0.05
0.03
0.01
0.005

b)

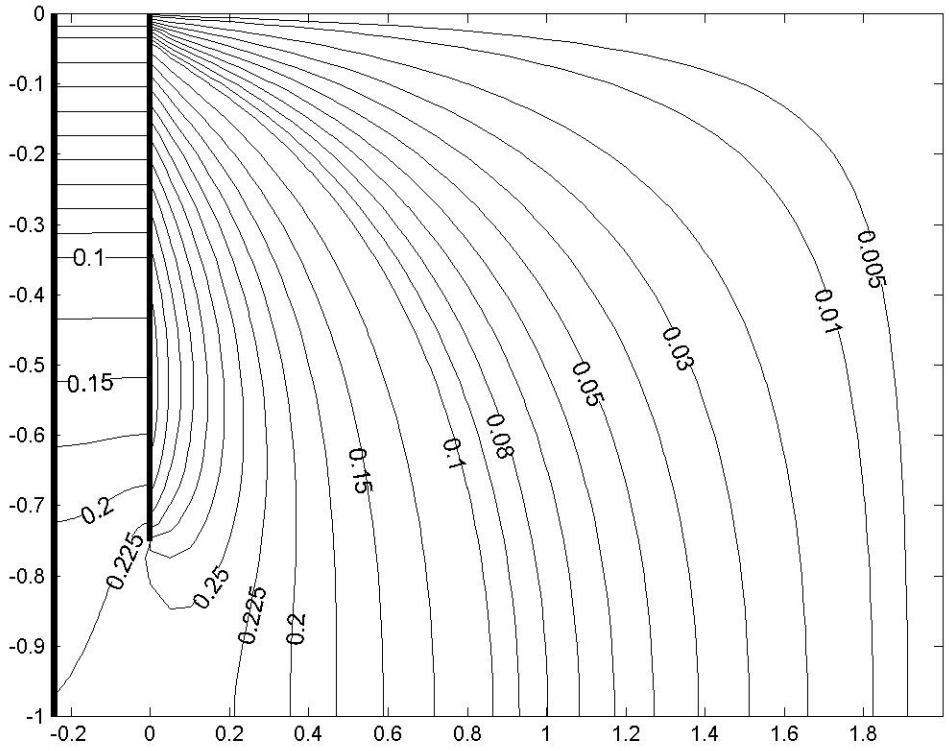

c)

Fig. 9 *P* due to wave impact on a baffle in front of a wall with b_1 = -0.25, H_b = 0.5; a) μ = 0.25, b) μ = 0.5 and c) with b_1 = -0.25, H_b = 0.75, μ = 0.75. The value of *P* on unlabeled closely-spaced contours is given by continuing the increment from neighbouring contour values.

The contours shown in Fig. 9 are spaced as in Fig.7. For b_1 = -0.25, H_b = 0.5, μ = 0.25 P_{max} is 0.14, for b_1=-0.25, H_b = 0.5, μ = 0.5 it is 0.26 and for b_1 = -0.25, H_b = 0.75, μ = 0.75 it is 0.42. Thus the effect of the rear wall is to increase these maxima compared to the corresponding baffle in open sea cases above.

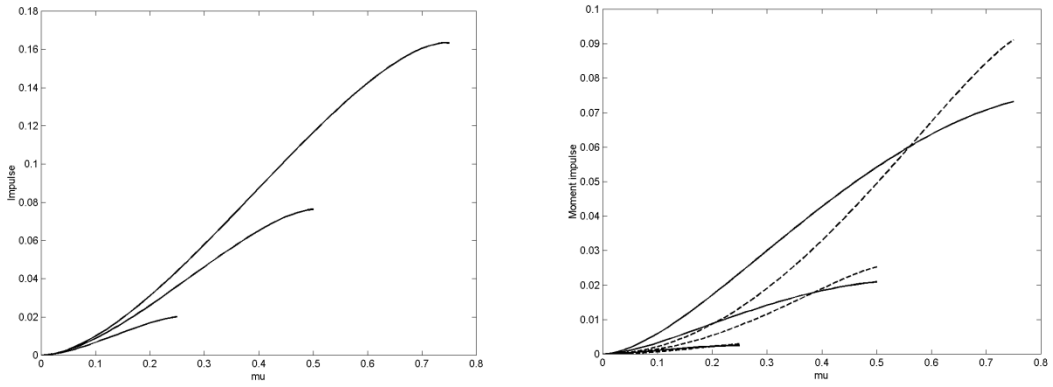

a) b)

Fig. 10 a) I due to wave impact on a baffle in front of a wall with b_1 = -0.25, H_b = 0.25, 0.5 and 0.75, and b) corresponding M values: solid/dashed line about the baffle bottom/top. For convenience of plotting, the negative of M about the top of the baffle is shown in the figure (as dotted lines).

Compared with the baffle in open sea case, Fig. 8, Fig.10 shows that there is about a 12% reduction in I and an increase in M taken about the bottom (top) of the baffle of about 10% (38%). As expected, we again see a monotonic increase in I and M as H_b increases.

6. Case 5: horizontal wave impact onto a surface-piercing vertical baffle in front of a wall with a deck extending from the wall to the baffle.

The eigenfunction expansion for region 1 is now

$$P_1(x,y) = C + \sum_{n=1}^{\infty} \alpha_n \cos(\gamma_n y) \frac{\cosh[\gamma_n(x-b_1)]}{\cosh(\gamma_n b_1)} \qquad [7]$$

where $\gamma_n = n\pi$ so that the deck condition is automatically satisfied. Similarly the cosh and the 'secular' terms C satisfy the wall condition. The eigenfunction expansion for region 2 is again given by eq. 3 and the solution procedure is similar to that above, whereby C is a summation with terms having coefficients α_n and c_n, and so, after truncation C can therefore be eliminated to again give an 2N x 2N system of equations, for details see Md Noar (2012).

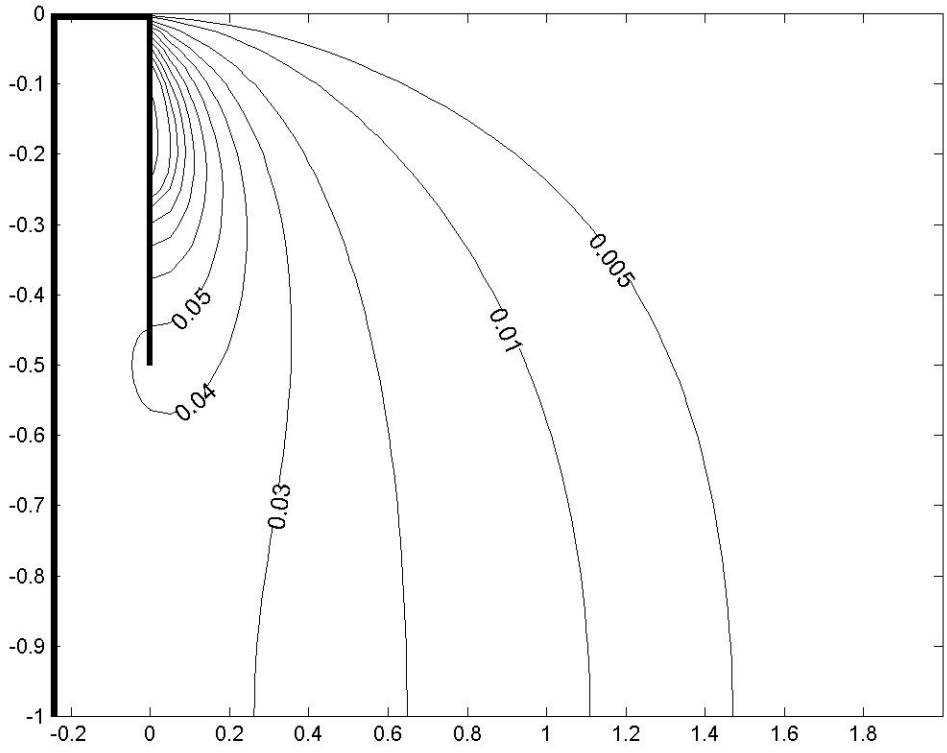
0
-0.1
-0.2
-0.3
-0.4
-0.5
-0.6
-0.7
-0.8
-0.9
-1
-0.2
0
0.2
0.4
0.6
0.8
1
1.2
1.4
1.6
1.8
0.05
0.04
0.03
0.01
0.005

a)

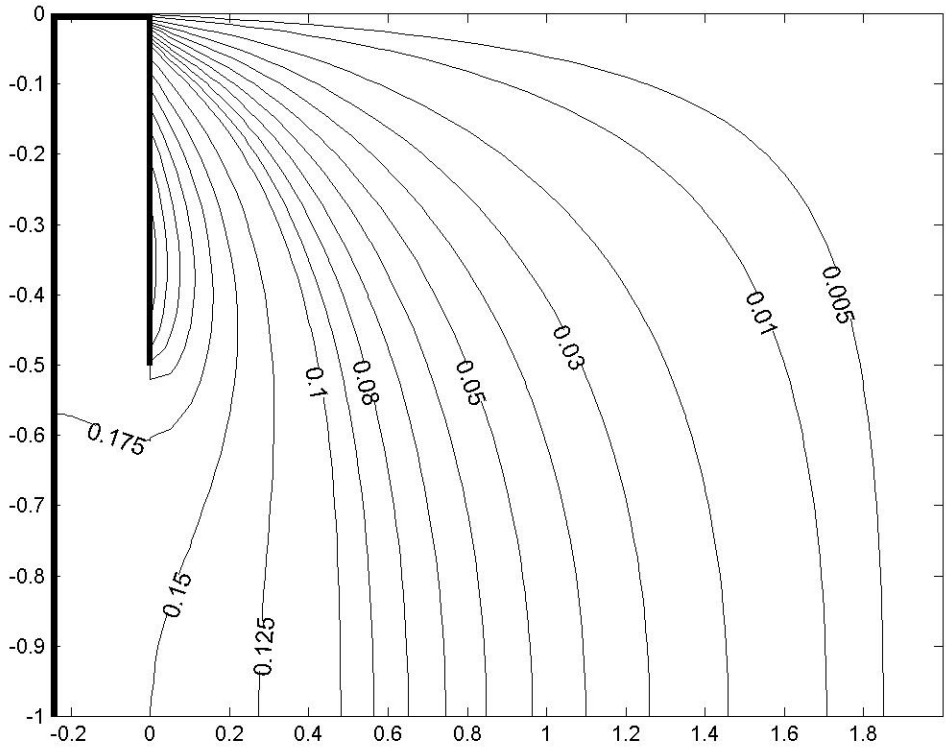
0
-0.1
-0.2
-0.3
-0.4
-0.5
-0.6
-0.7
-0.8
-0.9
-1
-0.2
0
0.2
0.4
0.6
0.8
1
1.2
1.4
1.6
1.8
0.175
0.15
0.125
0.1
0.08
0.05
0.03
0.01
0.005

b)

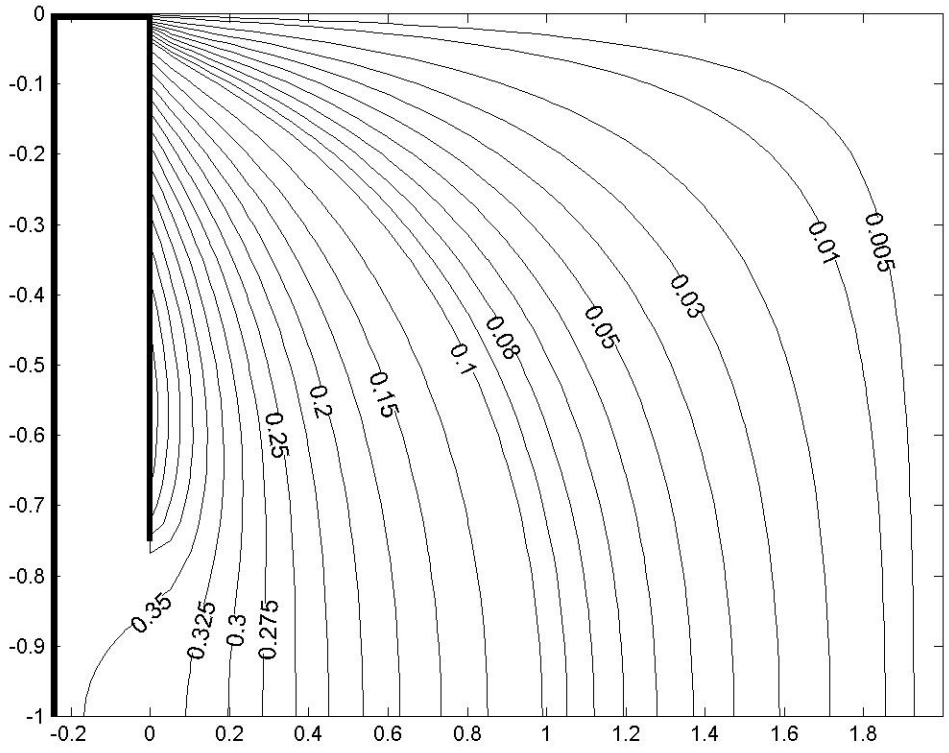

c)

Fig. 11 P due to wave impact on a baffle with in front of a wall with a deck b_1 = -0.25, H_b = 0.5; a) μ = 0.25, b) μ = 0.5 and c) with b_1 = -0.25, H_b = 0.75, μ = 0.75. The value of P on unlabeled closely-spaced contours is given by continuing the increment from neighbouring contour values.

The contours shown in Fig. 11 are spaced as in Fig. 7. For b_1 = -0.25, H_b = 0.5, μ = 0.25 P_{max} is 0.14, for b_1 = -0.25, H_b = 0.5, μ = 0.5 it is 0.29 and for b_1 = -0.25, H_b = 0.75, μ = 0.75 it is 0.47. Thus the effect of the deck is to increase these maxima compared to the corresponding no-deck case above.

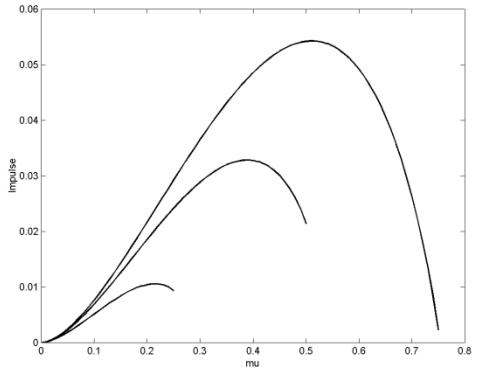

a)

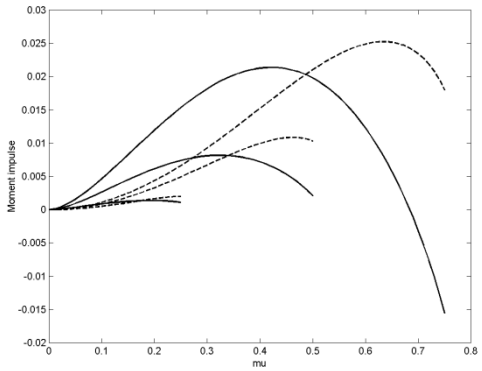

b)

Fig. 12 a) I due to wave impact on a baffle in front of a wall with b_1 = -0.25, H_b = 0.25, 0.5 and 0.75, and b) corresponding M values: solid/dashed line about the baffle bottom/top. For convenience of plotting, the negative of M about the top of the baffle is shown in the figure (as dotted lines).

Clearly the high values of P 'trapped' behind the baffle seen in Fig. 11 has a major effect on I and M. It can even reverse their direction for larger baffles so that with b_1 = -0.25, H_b = 0.95, the maximum I of 0.06 (i.e. backwards) occurs at μ = 0.55, whilst at μ = 0.95 it has a value of about -0.11 (i.e. forwards). A similar situation occurs for M, where with moment axis at the bottom the corresponding figures are 0.032 for the maximum and -0.96 for μ = 0.95, and with moment axis at the top, the corresponding figures are -0.031 for the minimum and 0.011 for μ = 0.95. Since the wave impacts from right to left, high initial pressure will certainly occur on the front face of the baffle but will propagate to the rear of the baffle during the impact. Here there is no free surface, so high P values will occur right up to y = 0, in contrast to the front face where there is a free surface and hence they decrease to a zero P at y = 0. Thus I on the rear of the baffle can exceed that on the front. Md Noar (2012) considers the individual wall, deck and baffle components of I and M about the bottom of the wall (0,-1) as well as that for the combined body, and also for I and M acting on the seabed.

7. Case 6: bottom-mounted baffle in front of a wall with impact occurring on the wall.

Since the wall (not the submerged baffle) is impacted, we here revert to the coordinate system of Fig. 1 with the baffle at $x = b_1$ and with $-1 < y < -H_b$. The eigenfunction expansion in region 1 is now:

$$P_1(x,y) = \sum_{n=1}^{\infty} \sin(\lambda_n y) \left\{ \alpha_n \frac{\sinh(\lambda_n (x-b_1))}{\cosh(\lambda_n b_1)} + \beta_n \frac{\cosh(\lambda_n (x-b_1))}{\cosh(\lambda_n b_1)} \right\} \qquad [8]$$

whilst in region 2, it is again given by Eq. 3.

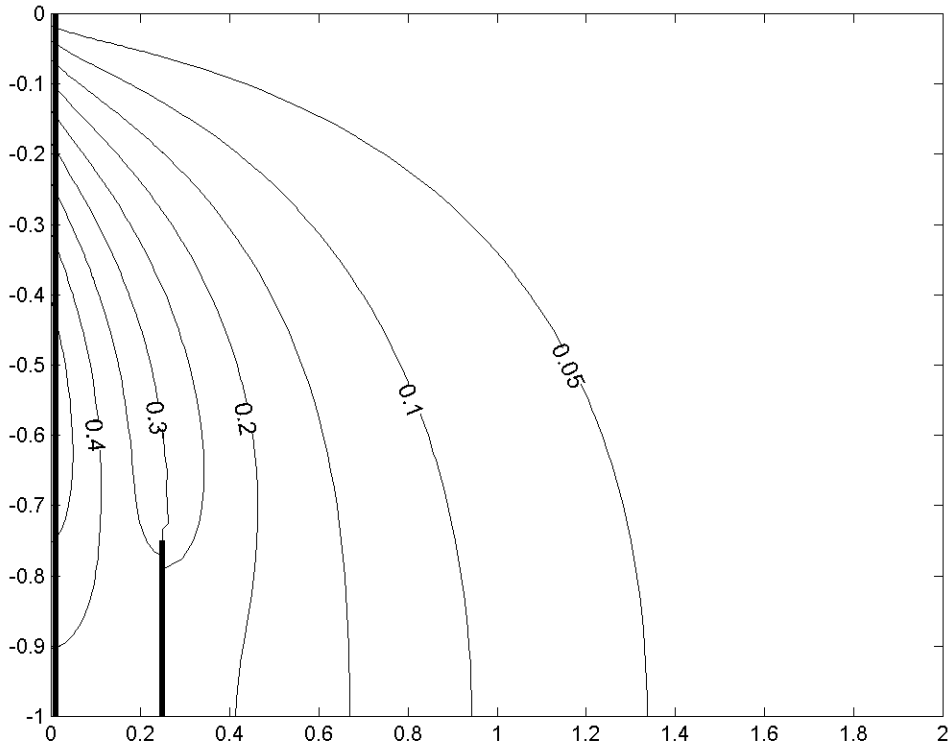
0
-0.1
-0.2
-0.3
-0.4
-0.5
-0.6
-0.7
-0.8
-0.9
-1
0
0.2
0.4
0.6
0.8
1
1.2
1.4
1.6
1.8
2
0.05
0.1
0.2
0.3
0.4

a)

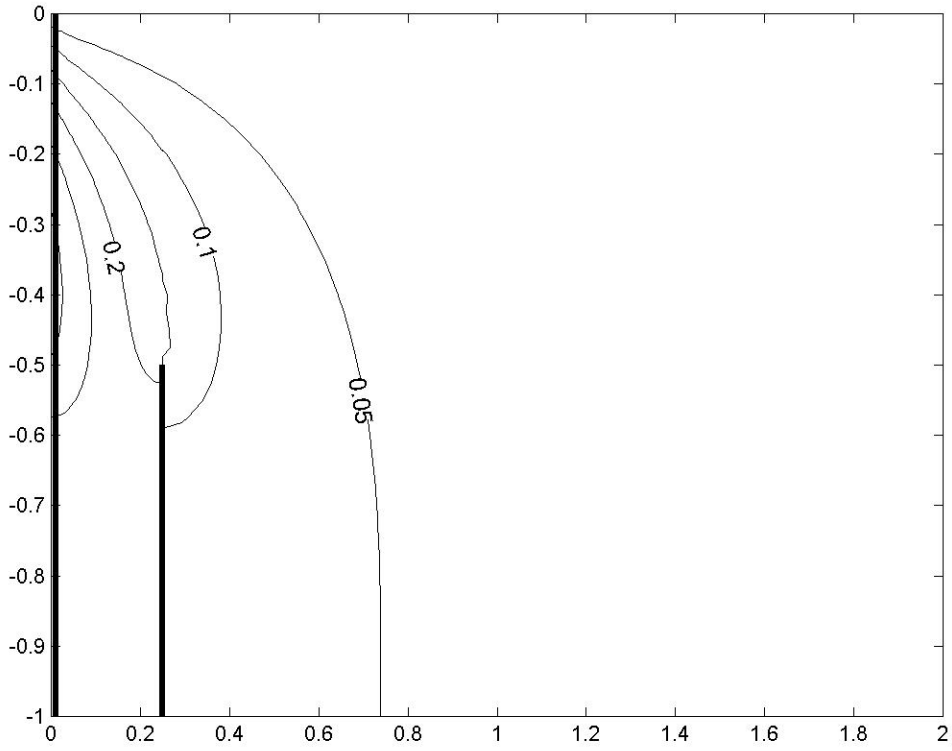

b)

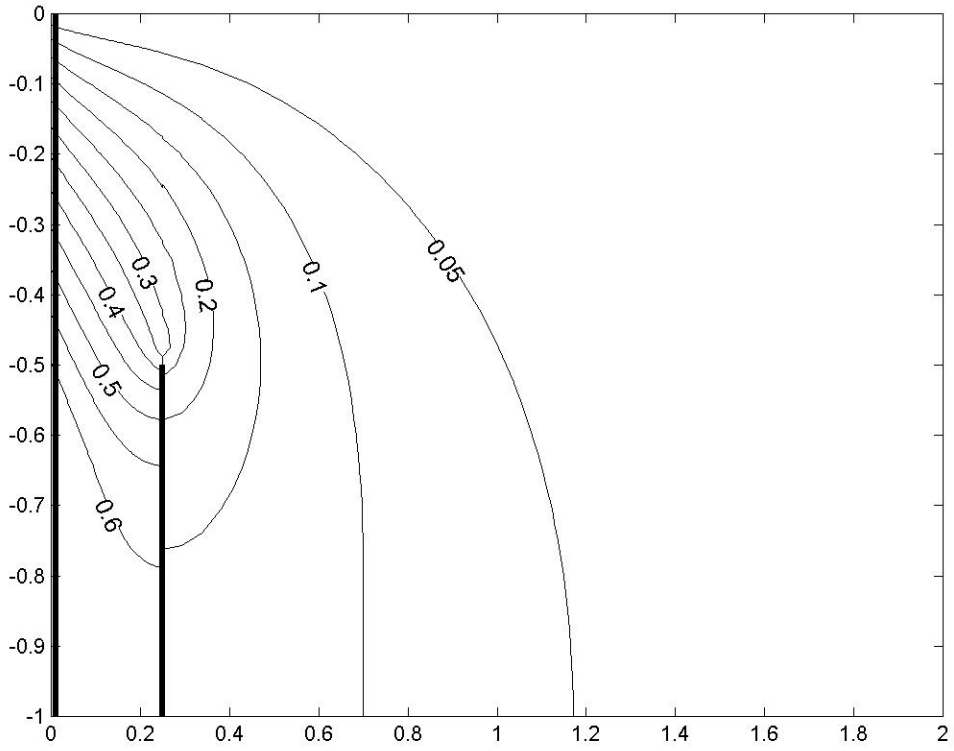

c)

Fig. 13 P due to wave impact on a wall with a bottom-mounted baffle. a) b_1 = -0.25, H_b = 0.75, μ = 0.75 and with b_1 = -0.25, H_b = 0.5; b) μ = 0.5 and c) μ = 0.75. The value of P on unlabeled closely-spaced contours is given by continuing the increment from neighbouring contour values.

Here we see high P being 'trapped' behind the baffle, a similar effect to that noted in part 1 for the ditch problem. The cases where $\mu > H_b$ seem unlikely to occur for wave impact in open sea, or for sloshing caused by horizontal tank motions, but may occur for a tank in angular motion caused by rolling or pitching of a ship. In that case, we imagine the wave to fall over the top of the baffle into an air-filled region behind it (which in itself may cause an air pocket to become trapped but this is ignored here). Such motion is known from the experiments reported in Peregrine *et al* (1999). For the baffle shown in Fig. 13 with b_1 = -0.25, this P_{max} on the wall is above the no-baffle case, increasing from 0.29 for μ = 0.5 and 0.47 for μ = 0.75, to 0.32 and 0.68 respectively, with a corresponding increase on the wall I and M, see Md Noar (2012). Here we focus on those quantities for the baffle, as shown in Fig. 14. Note that I acts in the positive x direction and M about the bottom/top of the baffle is negative/positive. The effect of a taller baffle (smaller values of H_b) is to 'trap' more effectively higher values of P against the wall so that I and M both increase, as shown in Fig. 14.

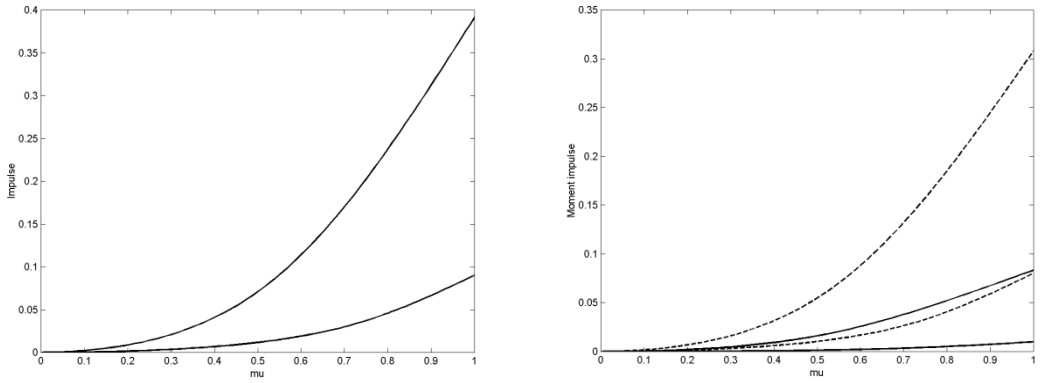

a) b)

Fig. 14 a) I due to wave impact on a baffle in front of a wall with b_1 = -0.25, H_b = 0.75 (lower graph) and 0.5 (upper graph), and b) correspondingly-increasing M: solid/dashed line about the baffle bottom/top. For convenience of plotting, the negative of M about the bottom of the baffle is shown in the figure (solid lines).

8. Effect of porous boundary conditions on a seawall/seabed/berm

We now consider the effect of porous boundaries on P throughout the fluid region (but not in the porous media), and consequent I and M. This study contrasts with that of Wood and Peregrine (2000) who considered P above and within a porous berm of such length that it has decayed to zero at the seaward end of the berm, so that no matching is required here. An alternative model that also considers flow within the porous media (modelled by a series of regularly place horizontal holes) was considered by Cooker (2013). In both models, porosity is shown to reduce the impact pressures and we here confirm that general conclusion.

We assume that in the fluid adjacent to a porous boundary, the boundary condition can be expressed by a Robin condition:

$$\frac{\partial P}{\partial n} - aP = 0 \qquad [9]$$

where n is the surface normal and a is a parameter that characterizes porosity of the wall a_w, the seabed a_s, the top of the berm a_b, or the front face of the berm a_f ($x = B_1$, $-H_b > y > -1$, see Fig 6 of part I of this paper). Given the impulsive nature of the impact, a_s is not easy to estimate but is likely to be higher than that given by usual groundwater or cyclical wave-induced liquefaction measurements, see Sumer (2014). However, we can give a rough estimate by assuming flow acts normally to the surface and the pressure decreases linearly to zero after distance L. Further, assuming Darcy's law we then have

$$u = \frac{K}{\mu_{vis}} \frac{p}{L} \qquad [10]$$

where u is the normal fluid velocity into the porous media, p is the pressure at the surface, K is the intrinsic permeability with estimates of porosity depending on the type of ground (gravel - sand) being in the range 10^{-7} – 10^{-11} m^2 and μ_{vis} (in eq. 10) is the dynamic viscosity (approximately 10^{-3} Pa s), as given by Bear (1972). On the other hand, the pressure impulse model gives:

$$u_a - u_b = -\frac{1}{\rho}\frac{\partial P'}{\partial n} \qquad [11]$$

see Lamb (1932). Here P' is the dimensional pressure ($P' = P\,\rho U_0 H$ as above) and u_a is the normal velocity after impact whilst u_b is that before impact, here assumed to be zero. Noting that this model integrates over the impact duration Δt, we assume that the mean value of u over the impact duration is comparable with its value after impact: thus we can equate eq. [10] and eq. [11], giving eq. [9] with dimensionless porosity parameter:

$$a = \frac{K\rho}{\mu_{vis}\,\Delta t}\frac{H}{L} \qquad [12]$$

Using the values for permeability and viscosity given above, and assuming a typical value of $\Delta t \sim 10^{-2}$ s and arbitrarily choosing $L = H$, we get values for a in the range 0-10, the higher value being for the most porous seabed comprising gravel. However, taking the value of the permeability estimated from steady-state conditions (as in groundwater calculations) or from cyclical wave-induced pressures is open to considerable doubt, since the impact is highly transient. It may indeed have more similarity to the situation reported by Hatzor *et al* (2009) where liquefaction due to explosions in saturated clay-rich sand deposits was measured in situations "not considered prone to liquefaction in standard liquefaction prediction procedures". Correct modelling of porosity is very problematic, especially since van Gent (1995) advocates Forchheimer equation that includes a quadratic term in velocity to model turbulence and/or flow separation within the porous medium. Such advocacy relies on experimental data and we must therefore view Forchheimer's equation as empirical; given the lack of experimental data for the impulsive situations considered here, it is therefore not clear that the inclusion of a quadratic form is justified, especially considering Hatzor *et al*'s comment above. Moreover, even if we were to do this in some sort of numerical model, it seems doubtful that measured coefficients of the linear and quadratic terms from oscillatory motion experiments would be applicable here. Molin and Korobkin (2001) and Iafrati and Korobkin (2005) do include a quadratic discharge law for the slamming impact of a permeable wedge and this suggests water entry experiments could establish the relative importance of linear and quadratic terms and determine their coefficients. We know of no such experiments, nor do we know if such results could be extended to the present cases (where experiments, probably conducted at large-scale to avoid scaling problems, would be far more challenging to do).

Despite the above uncertainties, the model proposed above, which has porosity parameter independent of the fluid velocity, is attractive since it allows linear superposition of

eigenfunctions used throughout this paper. This then allows rapid exploration of any porosity effects, albeit in an approximate way, hopefully to be compared with experiments and more sophisticated numerical results in the future. Even with our linearisation, calculation of a lies outside our model and must be supplied by suitable experimental measurements of impacts in the particular geometries we consider. We simply seek to encourage experimenters by showing that the effect of increasing a is potentially beneficial in reducing pressure impulse P throughout the fluid region. We note that a is a function of fluid and seawall and/or seabed material parameters, but also of Δt, so that, according to our model, shorter impact durations give lower values of P everywhere. However, in view of eq. [1] this does not mean that peak pressures p_{peak} will then decrease. For example, in comparing Fig. 15 c) having $a_s = 1$ with that for $a_s = 2$ (not shown), we find that the reduction in the maxima of P from circa 0.1 to only 0.09. This is insufficient to offset the doubling of p_{peak} estimated by eq. [1] and this may account for the liquefaction observed by Hatzor *et al* (2009). Wood and Peregrine (2000) report a reduction in P with increasing porosity, but their results focus on the seawall and not on the possible effect on the seabed also discussed here.

Eq. [9] can also be applied on the engineered structure (seawall and/or berm) where the engineer may be able to design in the required porosity by suitable choice of materials or construction techniques, for example using infill rocks behind a vertical screen in front of the breakwater, see for example Chwang and Chan (1998). Those authors compare Darcy's law with potential theory and demonstrate beneficial wave reducing effects due to such a construction. We show that from the point of view of wave impacts it could also be useful to engineer seawalls, berms and (in section 9) baffles with porous structures.

Let us first consider the impact of a wave on a porous vertical seawall with porosity parameter a_w above an impermeable seabed, with no berm. The eigenfunction expansion is given by:

$$P(x,y,\mu) = \sum_{n=1}^{\infty} c_n \sin(\lambda_n y) \frac{\sinh[\lambda_n(x-B)]}{\cosh(\lambda_n \mathbf{B})} \qquad [13]$$

as in part 1 of this paper but with the seawall boundary condition:

$$\frac{\partial P}{\partial x} - a_w P = \begin{cases} -1 & \text{for } -\mu < y < 0 \\ 0 & \text{otherwise} \end{cases} \qquad [14]$$

For a porous seabed and/or berm eq. [13] still applies but λ_n (chosen to satisfy impermeable conditions) must be replaced by ζ_n where

$$\zeta_n \cos(\zeta_n) + aH \sin(\zeta_n) = 0 \qquad [15]$$

Then each term of eq. [13] satisfies the porous boundary condition eq. [9] on the top of the berm ($B = B_1$, $H = H_b$ and $a = a_b$) or seabed ($B = B_2$, $H = 1$ and $a = a_s$), again see Fig. 6 of part I. Eq. [15] is easily solved using the Newton-Raphson method with $\lambda_n = (n - 1/2)\pi$ as start values. The summation in eq. [13] is truncated at $n = N$.

Convergence of P_{max} is rapid; for example, for the worst-case scenario of a impermeable seabed and the whole of a non-porous seawall being impacted, results are within 0.1% of its N=100 value at N=20. In the results presented here we typically use N=40.

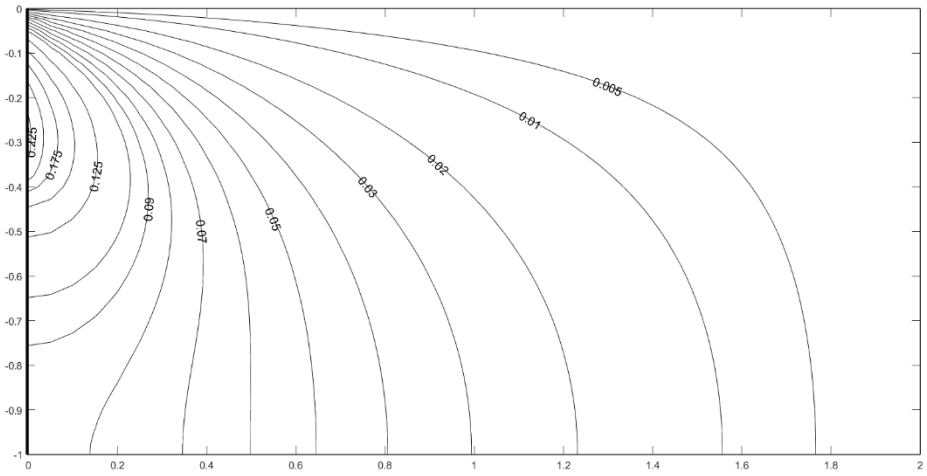

a)

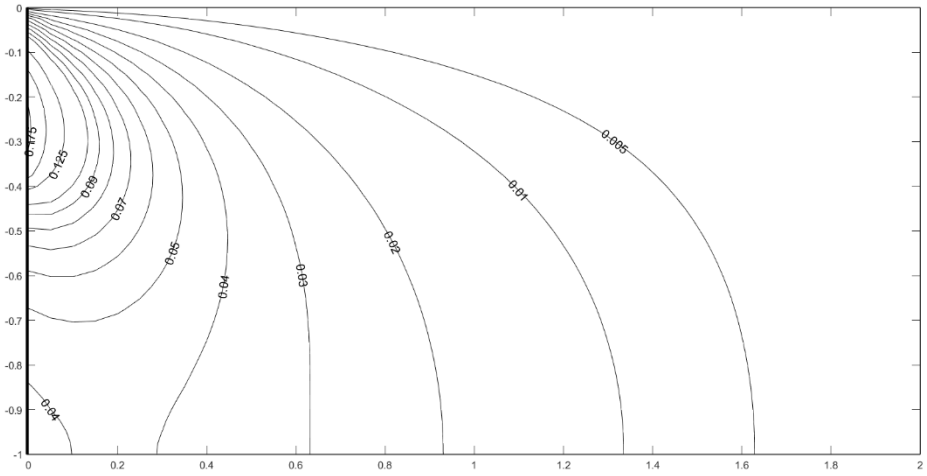

b)

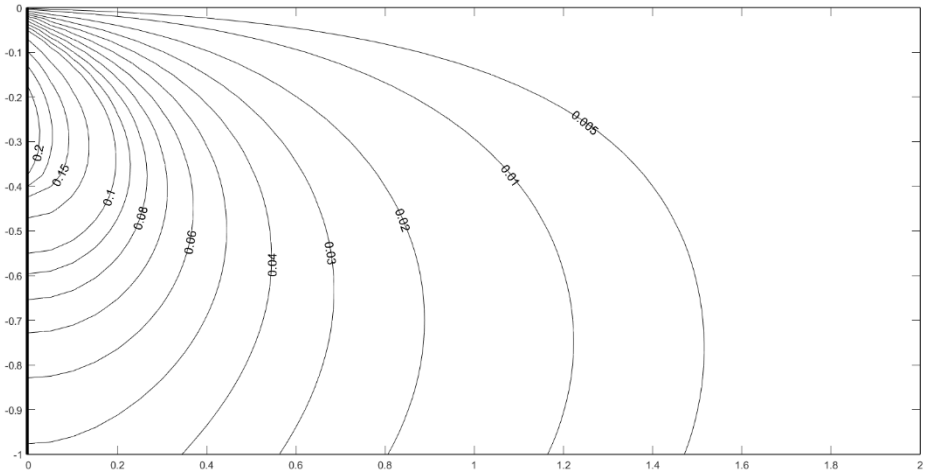

c)

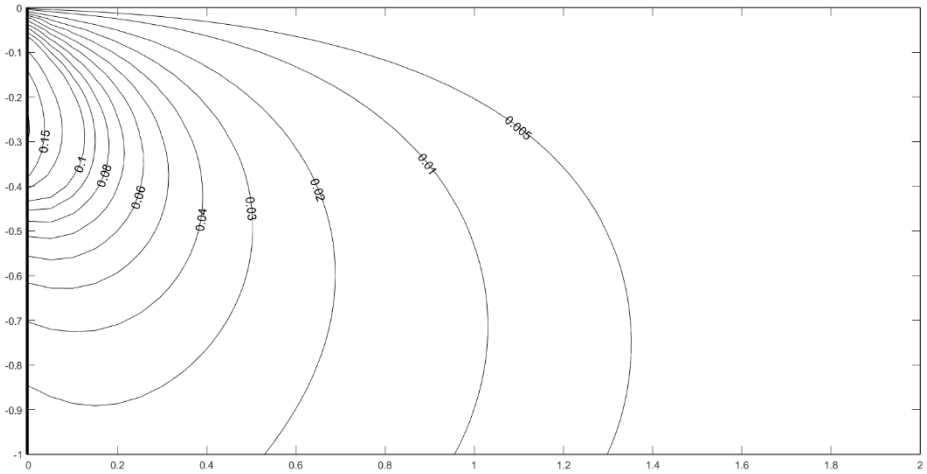

d)

Fig. 15 Pressure contours for μ = 0.4. a) an impermeable seabed and seawall (as in Fig. 2 of part I of this paper). b) an impermeable seabed but a porous seawall with $a_w = 1$. c) an impermeable seawall but a porous seabed with $a_s = 1$. d) a porous seawall and seabed with $a_w = a_s = 1$. The value of P on unlabeled closely-spaced contours is given by continuing the increment from neighbouring contour values.

Observe in Fig. 15 that for porous boundaries, contours of P are no longer normal (Note: for a) and c) the highest P contours are not sufficiently well resolved to show normality). Of more engineering interest is that porosity of either boundary, or both, causes a significant reduction in P_{max}, see Table 1, which occurs at a depth of around 0.3 in all cases. This means that its mean vertical gradient along the seawall is roughly halved for either $a_s = 1$ and $a_w = 1$, so that according to the uprush model of part I, the maximum

splash height attained will be reduced by a factor of about 4, thus predicting dramatically less overtopping.

P and its horizontal gradient at the seabed could be of considerable interest in determining whether or not seabed liquefaction occurs, but this lies outside the scope of this paper. Moreover, Cox and Cooker (1999) showed that the horizontal gradient is important for moving solid bodies (boulders) along the seabed for the impermeable case. Fig. 15 shows significant changes in the mean horizontal gradient with the impermeable case a) value being approximately 0.05, while the b), c) and d) values are all approximately 0.03. The corresponding values for $\mu = 0.8$ are 0.19, 0.11, 0.90 and 0.80 respectively.

We now consider the seawall extending to a depth of H_b, with a berm of horizontal extent B_1 as shown in Fig. 6 of part I. The seabed beyond the berm is impermeable (although calculations could be made to include this by modifying the eigenfunctions in region 2).

a_w	a_b or a_s	a_f	$\mu = 0.4$ no berm	$\mu = 0.4$ $B_1 = 0.2$ $H_b = 0.8$	$\mu = 0.6$ $B_1 = 0.2$ $H_b = 0.8$	$\mu = 0.8$ $B_1 = 0.2$ $H_b = 0.8$	$\mu = 0.4$ $B_1 = 0.4$ $H_b = 0.8$
0	0	0	0.230	0.232	0.365	0.561	0.234
1	0	0	0.179	0.181	0.259	0.368	0.183
0	1	0	0.227	0.226	0.345	0.477	0.244
0	0	1	-	0.229	0.355	0.533	0.234
1	1	0	0.177	0.179	0.251	0.330	0.180
0	1	1	-	0.225	0.338	0.461	0.245
1	0	1	-	0.180	0.255	0.355	0.181
1	1	1	-	0.178	0.248	0.322	0.178
2	0	0	0.150	0.151	0.203	0.273	0.151
0	2	0	0.220	0.223	0.333	0.438	0.207
2	2	0	0.148	0.150	0.197	0.240	0.150

Table 1 P_{max} for a seawall and a seawall with berm with different porosities resting on an impermeable seabed. Results for the impermeable wall and seabed considered in part I are shown for comparison (top row).

For $B_1 = 0.2$ and $H_b = 0.8$, for any porosity values on the wall or berm, the position of P_{max} stays roughly constant, being located at 0.3 down the seawall for $\mu = 0.4$, at 0.5 for $\mu = 0.6$ and at 0.8 for $\mu = 0.8$, and it decreases monotonically to the free surface. We note that in all these cases, the effect of porosity on the front face of the berm (at $x = B_1$) is weak; this implies that, from the point of view of P_{max}, the construction of the berm could be either caged porous material (e.g. rocks) or porous infill behind an impermeable retaining wall.

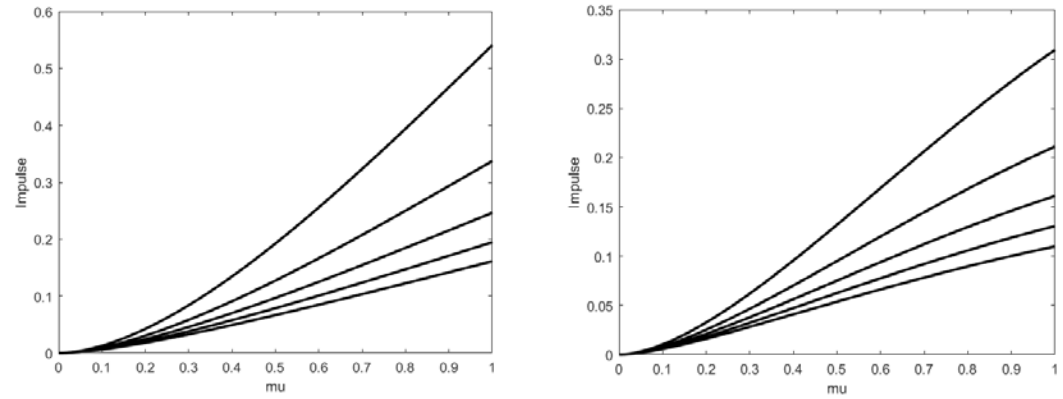

a) b)

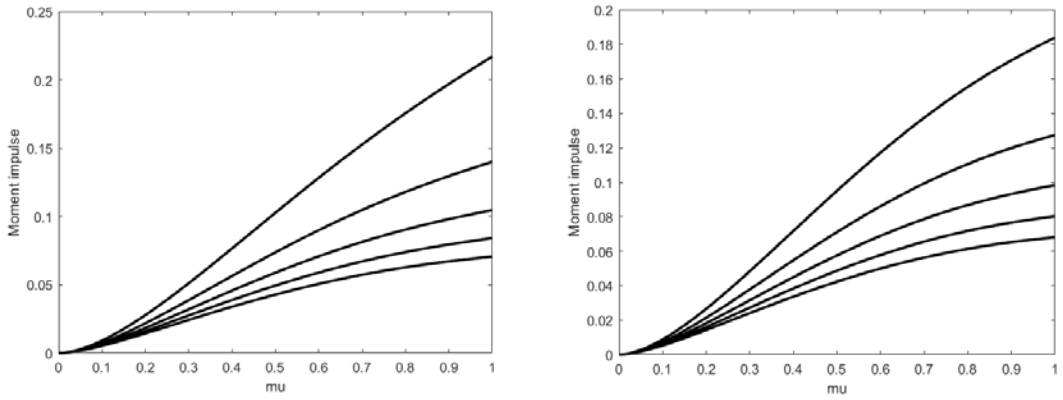

c) d)

Fig. 16 *I* on the seawall (no berm) for different porosities: a) impermeable seabed (i.e. a_s = 0) with a_w = 0, 1, 2, 3, 4 from top to bottom, b) as for a) but with a_s =1: c) and d) *M* (taken anticlockwise about x = 0, y = -1) corresponding to a) and b).

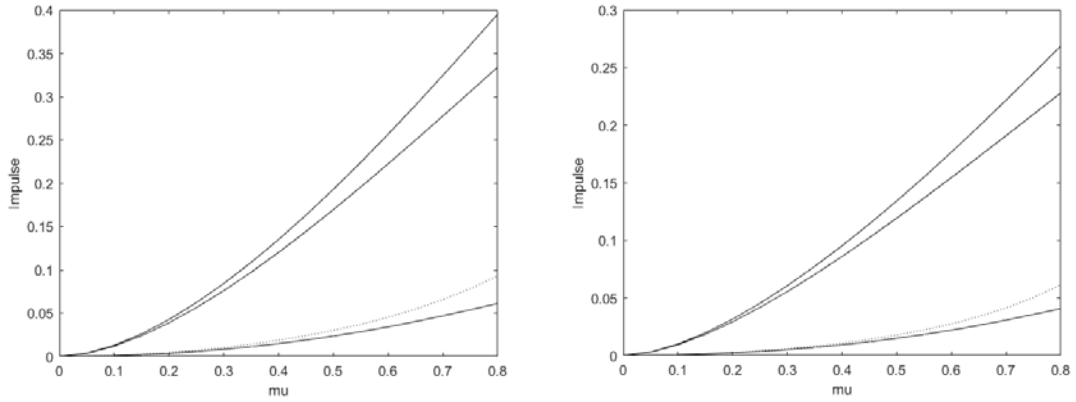

a) b)

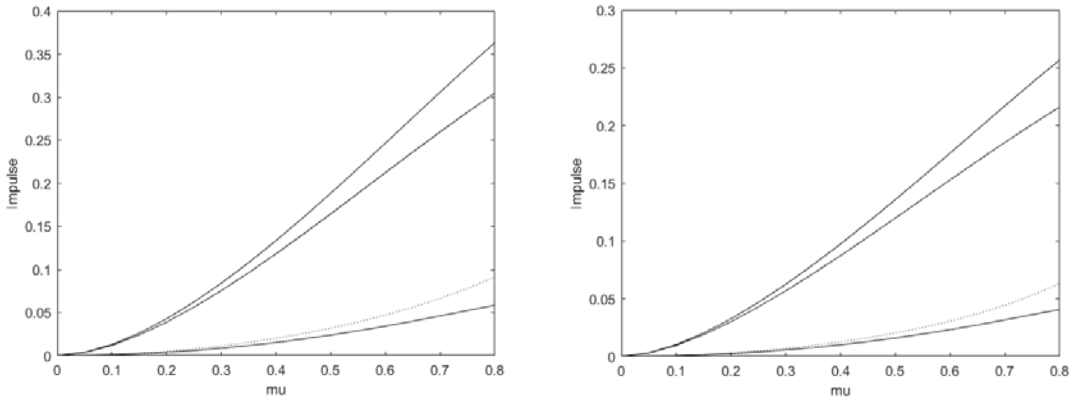

c) d)

Fig. 17 *I* on the combined seawall and berm with $B_1 = 0.2$ $H_b = 0.8$ for different porosities, as given in cases a)-d) in Fig.15. Solid lines (bottom to top) show landward impulse arising from the front face of the berm, the wall and the combination of the two, whilst the dotted line shows the downwards impulse acting on the top of the berm.

Given the reduction in the entire *P* field is greater for increasing wall porosity than for increasing berm porosity, it is not surprising that the horizontal impulse is markedly reduced; however, this is also true for the vertical impulse acting on the top of the berm. This may have engineering implications for the construction of seawalls; see below for comments on *I* and *M*.

a_w	a_b	a_f	$B_1 = 0.2$ $\mu=H_b=0.8$	$B_1 = 0.4$ $\mu=H_b=0.8$	$B_1 = 0.2$ $\mu=H_b=0.6$	$B_1 = 0.4$ $\mu=H_b=0.6$	$B_1 = 0.2$ $\mu=H_b=0.6$	$B_1 = 0.4$ $\mu=H_b=0.6$
0	0	0	0.173	0.154	0.120	0.111	**0.229**	**0.220**
1	0	0	0.120	0.107	0.093	0.084	**0.172**	**0.166**
0	1	0	0.155	0.132	0.115	0.099	**0.224**	**0.201**
1	1	0	0.112	0.096	0.088	0.077	**0.167**	**0.156**
1	1	1	0.109	0.095	0.083	0.075	**0.154**	**0.146**
2	0	0	0.092	0.082	0.074	0.067	**0.140**	**0.131**
0	2	0	0.140	0.116	0.104	0.090	**0.208**	**0.182**
2	2	0	0.082	0.070	0.068	0.059	**0.132**	**0.117**

Table 2 Extreme values of *M* taken about (0,-1), measured anticlockwise, and *I* in the landward direction (bold values in last two columns).

Table 2 shows porosity has a similar beneficial effect on the largest values *M* that occur in the extreme case when the entire seawall front is impacted. For smaller values of μ the values of *M* decrease almost linearly, so are not presented here. For all values presented here, the overturning moment has three components: on the seawall, on the top of the berm (a clockwise moment) and on the front face of the berm. For the cases presented here, the first is dominant, whilst the latter two are contribute 5-10% of *M*. For $H_b = 0.8$, the absolute values of clockwise moments on the berm top exceed those of the anticlockwise moments on the front, whilst for $H_b = 0.6$ the roles are reversed. This is to

be expected, since the moment arm is larger, but shows that increasing porosity of the seawall is more beneficial than increasing it for the berm.

Table 2 also gives extreme values of I in the landward direction with $H_b = 0.6$, whilst for $H_b = 0.8$, see Fig. 17. Note that even in this case where the front face of the berm comprises 0.4 of the water depth, having a porous front face reduces the value by less than 10% (for porosities of 2,2,2 in the first three columns, this value is 0.109).

9. A porous baffle

We now reconsider a vertical baffle in open ocean with an impermeable bottom, penetrating from the free surface to a depth H_b, case 3) shown in Fig. 6 above. The eigenfunctions are as before, but since the baffle has porosity parameter a_{baffle} the boundary conditions for P_1 and P_2 on the left and right side of the baffle are now assumed to be:

$$\frac{\partial P_1}{\partial x} - a_{baffle}(P_1 - P_2) = 0 \quad \text{for} - H_b < y < 0 \qquad [16]$$

$$\frac{\partial P_2}{\partial x} - a_{baffle}(P_2 - P_1) = \begin{cases} -1 & \text{for} - \mu < y < 0 \\ 0 & \text{for} - H_b < y < -\mu \end{cases} \qquad [17]$$

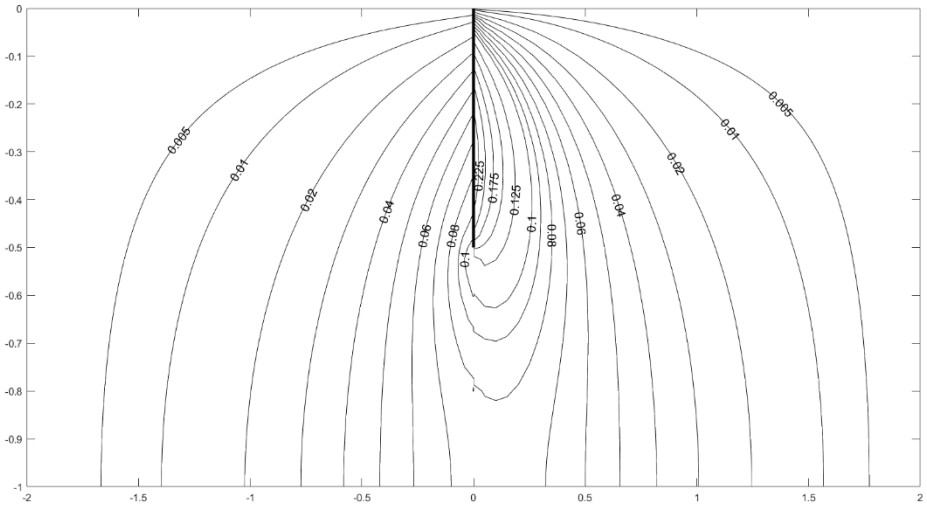

a)

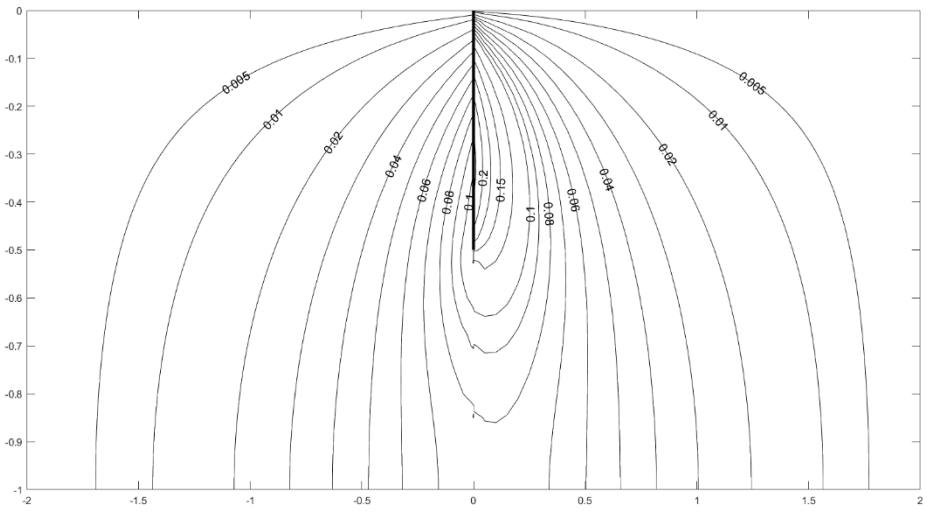

b)

Fig. 18 P due to wave impact on a baffle with $H_b = 0.5$ and $\mu = 0.5$. a) $a_{baffle} = 1$, b) $a_{baffle} = 2$. For $a_{baffle} = 0$ see in Fig. 7. The value of P on unlabeled closely-spaced contours is given by continuing the increment from neighbouring contour values.

It would be possible to consider porosity for the impermeable boundaries in any of the other cases (1-6), using modified versions of eqs. [14]-[17] depending on which surface is porous. The same comment applies to the case of unequal depths in regions 1 and 2; in a single wave impact one might expect the free surface in region 1 to be less than region 2, although this may not be true in a mixed sea or for sloshing in a baffled tank. Whilst this would merit further study, it would introduce another parameter into the problem so we have not done so; our focus here is to investigate how P, I and M are reduced by porosity. Fig. 18 shows that whilst P on the right-hand side of the baffle is not significantly affected (P_{max} for $a_{baffle} = 2$ is only decreased by about 10% from the $a_{baffle} = 0$ case), on the left-hand side it is significantly higher and this partial balancing effect reduces I and M, as shown in Fig. 19. Hyeon and Cho (2015) show that wave damping can be improved by having a porous baffle, reducing sloshing in normal operation conditions. Here we show that benefits from baffle porosity also occur in extreme situations where wave impact can occur.

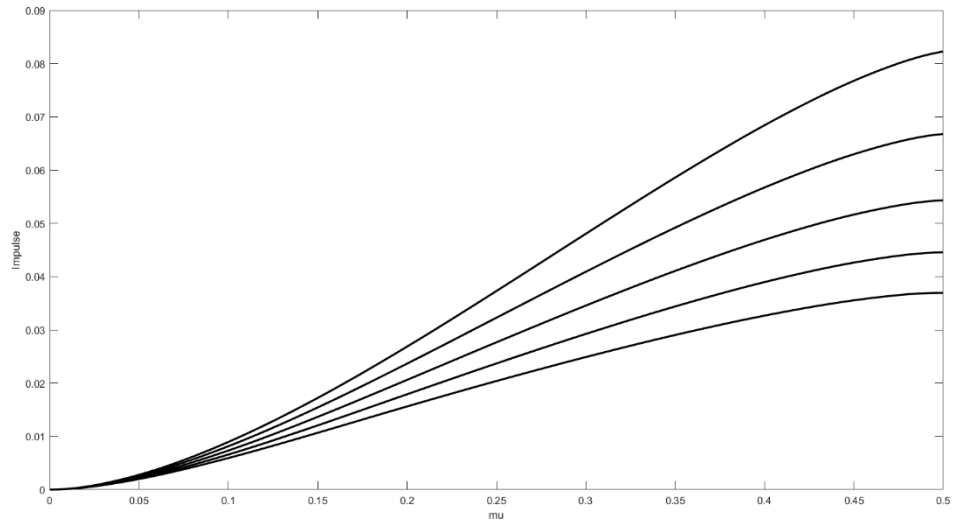

a)

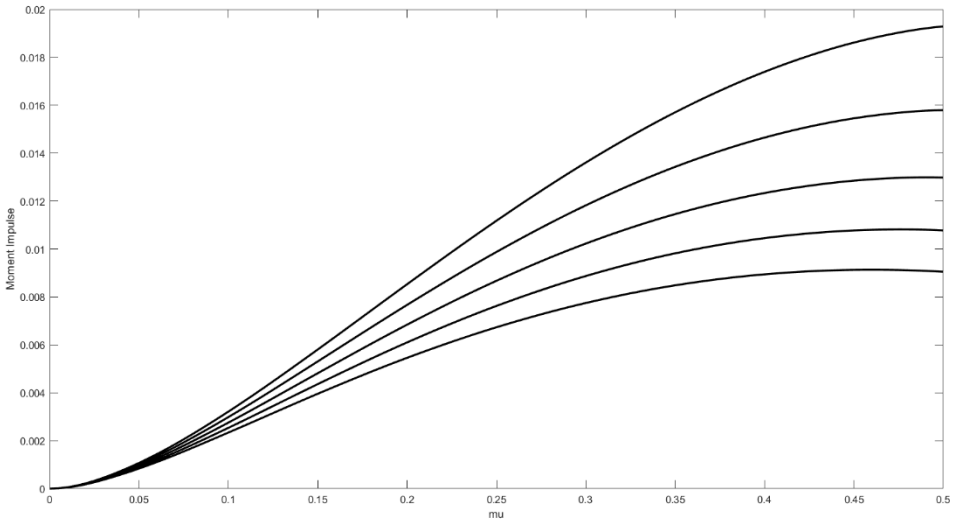

b)

Fig. 19 a) I due to wave impact with $H_b = 0.5$. b) M about the baffle top (0,0). Curves top to bottom are for $a_{baffle} = 0$, 1, 2, 3 and 4 respectively.

Conclusions

Given that the eigenfunctions used here automatically satisfy many of the boundary conditions, the satisfaction of the impact condition and matching of the two regions leads to a matrix equation of modest size for the unknown coefficients. Of interest in some cases is the inclusion of constant or spatially-linear secular terms, previously not needed in part I. Thus rapid exploration of the various models presented here is possible and might suggest suitable parameter ranges for fully nonlinear calculations or experiments.

In general, the inclusion of additional impermeable boundaries will increase *P* and thus significantly alter (and even reverse) *I* and *M*. For the cases considered here, we find:

a) for horizontal wave impact onto a vertical wall with a deck at the waterline, *P* increases as deck length increases. This causes a significant increase in *I* and *M* on the wall and the deck.
b) for vertical wave impact under a deck in the same configuration, *I* and *M* on the wall and deck again increase with increasing deck length. The results are in good agreement with those of Wood and Peregrine (1996) and can be also compared with those due to a flat plate in infinitely-deep water, for which a very simple analytical solution exists. Agreement is good for *I* and *M* on the deck, but less good for the wall.
c) for horizontal wave impact onto a surface-piercing vertical baffle in open sea, significant values of *P* can occur at the back of the baffle, causing a reduction in *I* and *M* compared with the wall case. Convergence to the wall case as baffle length increases is exceptionally slow for *M*.
d) for wave impact on a baffle in front of a wall with a free-surface between them, *P* behind the baffle increases compared to that of case 3) above. This can reduce *I* but increase *M*.
e) for wave impact on a baffle in front of a wall with a deck between them, high values of *P* can be 'trapped' behind the baffle which has a major effect on *I* and *M*.
f) for a bottom-mounted baffle in front of a wall with impact occurring on the wall, high values of *P* can again be 'trapped' behind the baffle, causing an increase *I* and *M* on the wall. The corresponding values on the baffle are also not small, even though the baffle is submerged and not directly impacted.

The present method can also accommodate modified boundary conditions intended to model porosity. For a seawall, with or without a berm, we see that seawall porosity has more effect than seabed porosity for *P*, *I* and *M*, although both are beneficial. Given the reduction of the vertical gradient of *P* near the seawall, the model of part 1 would predict significantly less overtopping. Values of *P* on the seabed could be important for the integrity of the seawall foundations since they provide suitable boundary conditions for modelling *P* within porous seabed media. Its horizontal gradient is also important for impact-induced motion of bodies on the seabed, see Cox and Cooker (1999). All of the above could be important in seawall design and construction.

We examined the effect of porosity on the impact on a baffle in open ocean. Although *P* on the impacted side of the baffle is reduced only slightly, the back side of the baffle experiences significantly higher *P*; this partially balances that on the impacted side and significantly reduces *I* and *M*, an effect that engineers may be able to exploit when designing anti-sloshing baffles.

Given the large number of geometric, dynamic and porosity parameters, general conclusions and overarching physical insights cannot yet be drawn from the limited number of cases presented. Indeed, our results highlight the significant effect of varying

geometry or boundary conditions, making estimation of P, I and M for unstudied cases problematic. It therefore seems necessary at this stage for engineers to do bespoke calculations for the specific cases required, and with more sophisticated models in non-rectangular geometries where the present techniques cannot be applied. Rather, we offer our results as benchmarks to be compared with further numerical or experimental studies. We stress again the desirability that experimentalists report the geometry and dynamics of the impact region itself, so that the current results can be validated, or otherwise. All we can say is that our results show that for the cases considered, the inclusion of additional impermeable boundaries increases P and thus significantly alters (and even reverses) I and M, whilst porous boundaries always reduce the severity of P, I and M. However, without further studies and validation, adoption of the above as general rules, and certainly application of our results in wider coastal and marine engineering contexts is not yet justifiable.

List of principal symbols

The geometrical parameters are defined in Fig. 1 with the exception of H_b which is the depth of the baffle bottom (or top in case 6). All geometrical parameters are non-dimensionalised by the water depth H.

a is the linear porosity parameter (defined in Eq. [12]); a_w refers to the seawall, a_s to the seabed and a_{baffle} to the baffle.

P, I and M are the dimensionless pressure impulse, impulse and moment impulse respectively (see Introduction). Physical quantities (denoted by a prime) are: $P' = P\,\rho U_0 H$, $I' = \rho U_0 H^2 I$ and $M' = \rho U_0 H^3 M$ where U_0 is the (assumed constant) normal (i.e. horizontal) impact velocity.

Δt impact duration.

μ depth of impact region, see Fig. 1.

Acknowledgements

The authors thank Dr Mark Cooker, University of East Anglia, UK and Dr Guido Wolters, Deltares, The Netherlands and the referees for their valuable comments.

References

Bear, J. (1972) *Dynamics of fluids in porous media.* Dover, 1988. ISBN: 0486656756. See also: https://en.wikipedia.org/wiki/Permeability_(earth_sciences) accessed 2018.

Brizzolara, S. *et al* (2009) Comparison of experimental and numerical sloshing loads

in partially filled tanks *Analysis and Design of Marine Structures – Guedes Soares & Das (eds)* Taylor & Francis Group, London, ISBN 978-0-415-54934-9 http://eprints.soton.ac.uk/68613/1/MASTRUCT-002.pdf accessed 1/8/2015.

Chan, E.S. and Melville, W.K. (1988). Deep-water plunging wave pressures on a vertical plane wall. *Proc. R. Soc. Lon.*. **417** 95-131.

Cooker, M.J. (1990). The interaction between steep water waves and coastal structures. *Ph.D Thesis* University of Bristol.

Cooker, M.J. (2013). A theory for the impact of a wave breaking onto a permeable barrier with jet generation. *J. J Eng Math* **79** 1: 1-12.

Cooker, M.J. and Peregrine, D.H. (1990). A model for breaking wave impact pressures. *Proc. 22nd Intl. Conf. Coastal Eng*. 1473-1486.

Cooker, M.J. and Peregrine, D.H. (1995). Pressure-impulse theory for liquid impact problems. *J. Fluid Mech.* **297** 193-214.

Cox, S.J and Cooker, M.J. (1999). The motion of a rigid body impelled by sea-wave impact. *Appl. Ocean Research.* **21** 113-125.

Chwang A.T. and Chan A.T. (1998) Interaction between porous media and wave motion. *Ann. Rev. Fluid Mech.* **30** 53-84.

Chen, X. *et al* (2019) Use of impulses to determine the reaction force of a hydraulic structure with an overhang due to wave impact. *Coastal Engineering*, **147** 75–88.

Faltinsen, O. M., Rognebakke, O. F. (1999) Sloshing and slamming in tanks. HYDRONAV'99-MANOEUVERING'99 Gdansk-Ostrada, Poland.

Faltinsen, O.M and Timokha, A.N. (2014) Sloshing. CUP ISBN 9781107646735.

Hatzor, Y.H., Gvirtzman, H, Wainshtein, I. and Orain, I. (2009) Induced liquefaction experiment in relatively dense, clay-rich sand deposits. *J Geophysical Res.* **114** B2 1-22.

Hofland,B., Kaminski, M.L., Wolters, G., (2010) Large Scale Wave Impacts on a Vertical Wall 32nd Int. Conf. on Coastal Engng, ICCE 2010, Shanghaï, China.

Hyeon, J-W. and Cho I-H. (2015) Experimental Study on Sloshing in Rectangular Tank with Vertical Porous Baffle. *J Ocean Eng. Tech.* **29** 4, 291-299.

Kim, Y. (2001) Numerical solution of sloshing flows with impact load *Appl. Ocean Res.* **23**: 53-62.

Kisacik, D., Troch, P. and van Bogaert, P. (2012) Experimental study of violent wave impact on a vertical structure with an overhanging cantilever slab *Ocean Engng*. **49**, 1-25.

Kisacik, D., Troch, P., Van Bogaert, P. and Caspeele R. (2014) Investigation of uplift impact forces on a vertical wall with an overhanging horizontal cantilever slab. *Coastal Engineering*, **90**, 12–22

Koli, G.C. and Kulkarni, V.V. (2010) Simulation of Fluid Sloshing in a Tank World Congress on Engineering Vol II, London.

Lamb, H. (1932) "Hydrodynamics" 6th ed. CUP.

Md Noar, N. A. Z. (2012) Wave impacts on rectangular structures. *PhD thesis*, Brunel University.

Md Noar, N. A. Z. and Greenhow M. (2015) Wave impacts on coastal structures with rectangular geometries: Part 1 Seawalls, *Appl. Ocean Res.* **53** 132-141.

Ming, P. (2010) Numerical simulation of sloshing in rectangular tank with VOF based on unstructured grids J. Hydrodynamics 2010,22(6):856-864 DOI: 10.1016/S1001-6058(09)60126-8 http://www.icname.org/upfiles/sci/p18.pdf accessed 1/8/2015.

Molin B. and Korobkin A. A. (2001) Water entry of a perforated wedge. Int. Workshop on Water Waves and Floating Bodies http://www.iwwwfb.org/Workshops/16.htm accessed 12/12/2018

Iafrati A. and Korobkin A. A. (2005) Self-similar solutions for porous/perforated wedge entry problem. Int. Workshop on Water Waves and Floating Bodies http://www.iwwwfb.org/Workshops/20.htm/ accessed 12/12/2018

Peregrine, D.H, Wood, D.J., Walkden, M. and Bruce, T. (1999) Pressure near wave impacts and the role of trapped air. Int. Workshop on Water Waves and Floating Bodies http://www.iwwwfb.org/Abstracts/iwwwfb14/iwwwfb14_32.pdf accessed 12/12/2018

Sumer, B. M. (2014) Liquefaction around marine structures. Adv Series on Ocean Engineering **39**. World Scientific.

Van Gent, M.R.A.(1995) Wave interaction with permeable coastal structures, PhD thesis, TU Delft, Netherlands.

Wagner, H. (1932) Uber Stoss- und Gleitvorgange and der Oberflache von Flussigkeiten. Z.A.M.M **12** 193-235.

Wang, W. and Xiong, Y. (2014) Minimising the sloshing impact in membrane LNG tank using a baffle. Proceedings of the 9th International Conference on Structural Dynamics, EURODYN 2014, Porto, Portugal.

Wood, D.J. and Peregrine, D.H. (1996). Wave impact beneath a horizontal surface. *Intl. Conf. on Coastal Eng*. Orlando, ASCE, **3** 2573-2583.

Wood, D.J. and Peregrine, D.H. (2000). Wave impact on a wall using pressure-impulse theory. II Porous berm. J Waterway, Port, Coastal and Ocean Engng. **126** 4 191-195.